A
Thesis
on

Optimization of synthesis parameters to obtain NbB_2 nanopowder at low temperature

Submitted in the fulfilment of the requirements for award of degree of

Master of Technology

in

Metallurgical and Material Engineering

(2016-2017)

Submitted by

Varun Singhal

(601502006)

Under the guidance of

Dr. O. P. Pandey

(Senior Professor)

School of Physics and Materials Science,

Thapar University

Patiala (Punjab)-147004

July 2017

Table of contents

Certificate

This is to certify that this dissertation entitled '***Optimization of synthesis parameters to obtain NbB_2 nanopowder at low temperature***' which is being submitted by ***Mr. Varun Singhal (601502006)*** in fulfilment of the requirements for the award of the degree of Master of Technology in Metallurgical and Material Engineering from School of Physics and Materials Science, Thapar University, Patiala, (Punjab), India is an exclusive record of candidate's own research work under the supervision of **Dr. O.P. Pandey**. The dissertation in part or in full has not been submitted in any other university or institute for the award of any degree.

Dr. O. P. Pandey
(Supervisor)
Senior Professor
School of Physics and Materials Science,
Thapar University, Patiala

Acknowledgement

After an extensive period of six months, I take this opportunity to write this note as a final touch of dissertation to express my gratitude and acknowledge the individuals who have helped for me in the completion of my thesis. These past few months were intense for me not only in the scientific but also on a personal level. The realm of time has taught me a lot and this dissertation has had a big impact on me. I would like to commence by thanking the people who helped throughout this period.

Prima face, I would like to thank my mentor and guide **Dr. O. P. Pandey** (Senior Professor, School of Physics and Materials Science) for his valuable guidance and constant support throughout the course of this work. He is the one who envisioned this project and deemed me worthy of doing this work. I thank him for his constructive criticism and the patience he has shown towards me. I would also like to thank **Mr. Aayush Gupta** for embarking on this journey with me and staying with me till the end, no matter how I felt, he was there for me throughout. Whenever I got stuck somewhere he is the one who helped me pull out of the situation and with such ease. He has been a friend, an elder brother and my co-mentor who believed in me more than I believed in myself and I thank him from all my heart.

It is my privilege to thank **Prof. Prakash Gopalan**, Director, Thapar University, Patiala, for providing the resources for my research work.

I would also like to thank **Dr Puneet Sharma**, **Dr. B. N. Chudasama**, **Dr. Loveleen Kaur Brar, Dr. N. K. Verma**, **Dr. Manoj Sharma** (Head SPMS) for their valuable support and help throughout the dissertation. I would also like to thank **Mr. Indermani Mishra**, **Mrs. Neelam Sadana, Mr. Purshottam Singh, Mr. Jant Singh** and **Mr. Pardeep Singla** for helping me at various times. I would like to extend my thanks to **Mr. Ghanshyam Morya** and **Mr. Mukesh Aggarwal** at SAI labs for their help.

My lab mates at functional materials lab, were my constant source of encouragement and so I would also like to thank them, **Dr. Gurbinder Kaur, Mr. Savid Khan, Mr. Rameez Mir, Mr. Piyush Sharma, Ms. Rupinderjeet bains, Mr. Amit Singh Vig, Ms. Harneet Kaur, Ms. Taranpreet Kaur, Mr Sachin jadika and Mr Navdeep kumar singh.** Thank you for being there in all the ups and downs.

I find this an opportune time to thank all my friends from whom I have gained a lot. It is because of them that I have learned how to be strong, firm and take a stand for myself.

Finally, I want to express my deepest gratitude to GOD, My Parents and My brother, to provide me support, help, big encouragement and lots of love. I am also proud to have the blessings of my Nani at every turning point of my life.

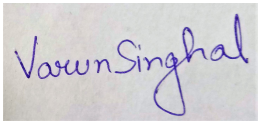

Varun Singhal

List of Figures

List of Tables Page

1. Introduction

Transition metals (TMs) of group V-VI have attracted many scientists from the early 19th century due to their good thermal, chemical and mechanical properties. TMs are being used in combination with boron, nitrogen and carbon as borides (TMBs), nitrides (TMNs) and carbides (TMCs) in various engineering sectors. Now a days, TMBs are being used as thermocouple elements in industries due to their high thermal stability [1]. Moreover, transition metal oxides (TMOs) and nitrides (TMNs) are used in the form of refractory components in aerospace industries for their excellent thermal and wear stability [2]. Boron is a brittle element which causes catastrophic failure of engineering components, while combination of boron with TMs can modify the various properties. Such combination can revolutionize the engineering sector, hence TM diborides are quite interesting category of materials with interesting mechanical and chemical properties.

1.1. Transition metal diborides (TMDBs)

Transition metal diborides are used over a wide range of applications based on their mechanical properties and refractory nature such as cutting tools and abrasives. In recent years, TMDBs are being used in rocket nozzles due to the fact that they have good thermal stability. These are known for their high strength and durability and hence, they are used under extreme conditions of temperature and pressure. Due to their high value of hardness, they find applications in cutting tools. The word *'refractory'* defines a material which possesses high melting point and can withstand heat at high temperatures.

Most of the elements in the periodic table combines with boron to form diboride, which are further divided into several categories depending upon their structures and characteristics. Among these, only the interstitial and covalent diborides meet the refractory criteria which includes the diboride of groups IV, V and VI. H. Moissan had synthesized the most of the borides [3] by using metal oxide and different boron sources and other metallic and non-metallic compounds which are shown in figure 1.1.

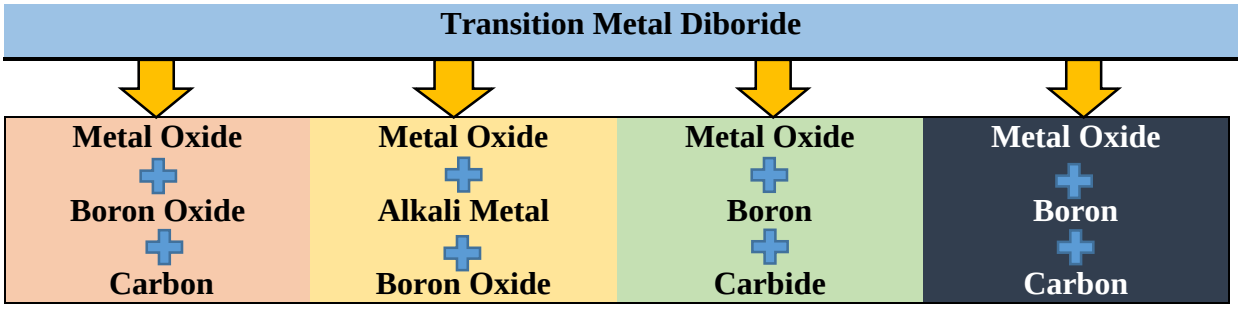

Figure 1.1: Preparation of transition metal diborides by H. Mooissan [4].

1.2. Physical properties of TM diborides

1.2.1. Nature of bonding

In the transition metal diborides, B-B bond is formed when a trivalent B atom shares an extra e^- with other B atom and formation of TM-B bond occurred when two extra e^- are provided by TM [1]. They have high wear resistance, high value of hardness, high elastic modulus, high melting temperature, good electrical and thermal conductivities. TM diborides shows good oxidation stability at high temperature and show corrosion resistant properties in 3d, 4d and 5d series of metal [1].

1.2.2. Crystal structure

AB_2-type A= {Ti, V, Cr, Zr, Nb, Mo, Hf, Ta, W} TMBs have P6/mmm space group (191) with a simple hexagonal crystal structure symmetry (D_6h). Instead of P6/mmm geometry, $R\bar{3}m$ and $P6_3/mmc$ geometry are observed in MoB_2 and WB_2, respectively due to the presence of puckered B layer [5,6]. Due to strong interlayer interaction, diborides are not complete layered compounds [7]. In the lattice vector of TMDBs, the atoms are positioned as TM (0,0,0), $B_1\left(\frac{1}{3},\frac{1}{6},\frac{1}{2}\right)$ and $B_2\left(\frac{2}{3},\frac{1}{3},\frac{1}{2}\right)$ in a unit cell. It forms a simple graphite like structure where boron atoms have a honey comb structure and TM atoms lie on the line passing in contiguous plane on through the center of boron [8]. Table 1.1 shows the crystal structure of various diborides and figure 1.2 shows schematic hexagonal crystal structure of diborides.

Table 1.1: Crystallographic parameters of TM and diborides [4].

TM	Structure	TMB	Structure	Space group
Titanium (Ti)	HCP	TiB_2	Hexagonal	P6/mmm
Zirconium (Zr)		ZrB_2		
Hafnium (Hf)		HfB_2		
Vanadium (V)	BCC	VB_2		
Niobium (Nb)		NbB_2		
Tantalum (Ta)		TaB_2		
Chromium (Cr)		CrB_2		
Molybdenum (Mo)		MoB_2		$R\bar{3}m$
Tungsten (W)		WB_2		$P6_3/mmc$

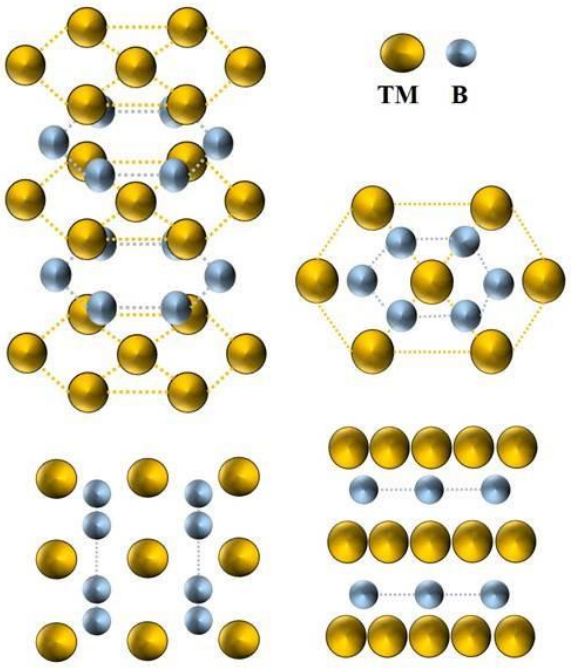

Figure 1.2: Crystal structure of AB_2-type structure.

1.2.3. Melting point

Melting temperature of TMs increases on going from Group IV to VI. Even after the formation of TMBDs, it follows same trend (figure 1.3). Hagg and Kiessling [9] explained that melting point increases as we go down the group which is contradictory to the fact that bond length increases down the group, so the bond strength weakens. But, it is also evident that the bonds determining the stability of diborides are not just TM-TM or B-B bonds. It's the combination of both so, it seems probable that the trend in the melting point primarily reflects the strength of TM-B bonds [3,10].

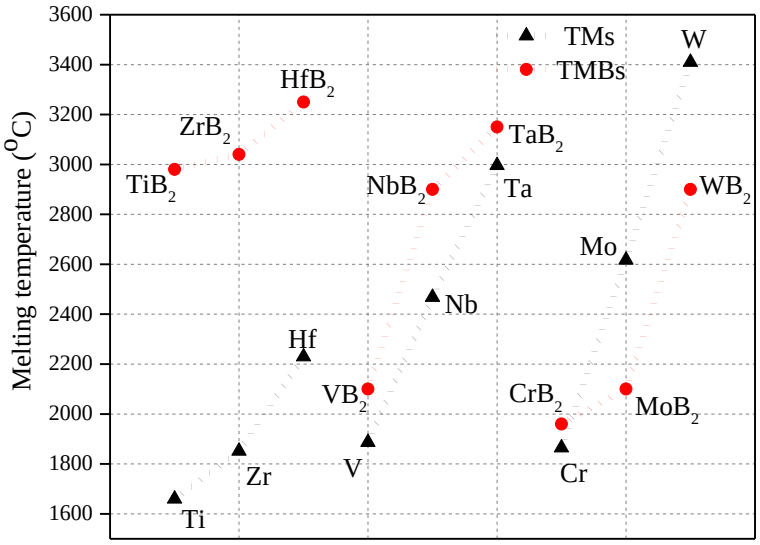

Figure 1.3: Melting points of various transition metal and their respective diborides.

1.2.4. Density

Group V and VI metals have BCC crystal structure but, group IV elements (Ti and Zr) have HCP structure. The transformation of TM to diborides causes the change in the crystal structure from HCP/BCC to simple hexagonal. Moreover, due to addition of boron, diborides are formed resulting the expansion of the unit cell. There's an appreciable increases in volume in comparison to its mass leading to decrease in the density of TMDBs as shown in figure 1.4.

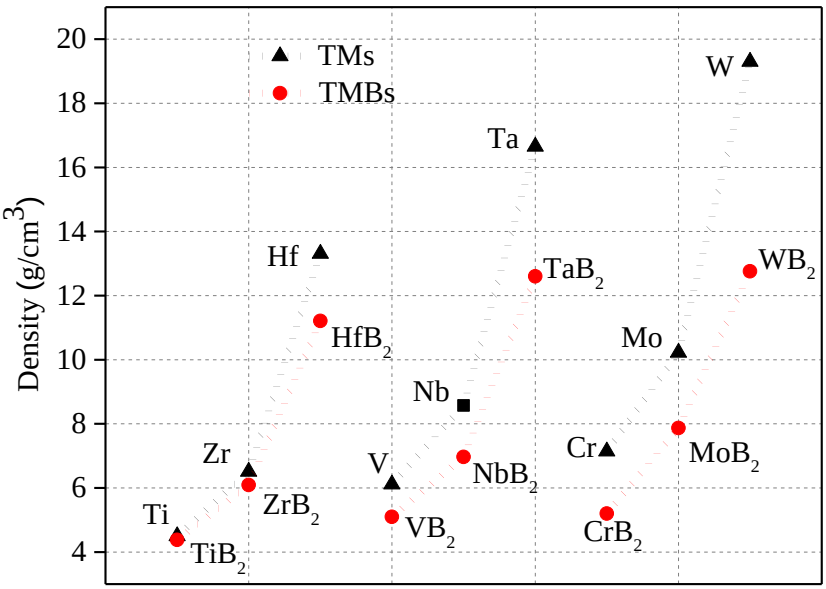

Figure 1.4: Variation in density of transition metals and their diborides.

1.3. Thermal expansion

Thermal expansion is a physical property that measures the change in the dimensions of a material with respect to temperature. Thermal expansion for bulk materials can be measured using a push-rod dilatometer [11]. Atoms have a lowest energy at 0 K from which increasing temperature results to increase in the energy of atom due to the atomic vibrations leading to inlargement of bond length and hence termed as thermal expansion. In strongly bonded boride, the amplitude of the vibrations is small which leads to smaller dimensional changes [12] hence, a reduced thermal expansion. Table 1.2 represents the variation in thermal expansion coefficients of group IV to VI TMBD. From whjich it can be observed that there is an increasing trend in group IV and V while, a decreasing trend in group VI.

Table 1.2: Magnitude of thermal expansion expansions of different TMDBs [13]**.**

TMDBs	TiB_2	ZrB_2	HfB_2	VB_2	NbB_2	TaB_2	CrB_2	MoB_2
Thermal expansion coefficients $\times 10^6$ /°C	4.6	5.9	6.3	7.6	8.0	8.2	10.5	7.7

1.4. Mechanical properties

The materials which are used in different industrial applications have different types of forces acting on them in all the directions. These forces is measured in the form of strength, hardness, toughness etc. Generally, the mechanical properties of TMDBs depend on some of the factors which are enlisted below:

1. Stoichiometry composition of TM and boron resulting TMDBs.
2. Grain size and morphology of sintered sample.
3. Presence of different phases.
4. Presence of impurities.

1.4.1. Elastic constants

Elastic constants govern different elastic properties of crystals such as elastic modulus, bulk modulus, poisson ratio and strain energy etc. For a hexagonal crystal structure, five independent elastic constants, termed as C_{11}, C_{12}, C_{13}, C_{33} and C_{44}, decide the magnitude of above mentioned elastic properties. Hill [14] and Kittel [15] suggested some mathematical relationships of elastic constants for various diborides which define the mechanical stability of unit cell. These stability conditions for hexagonal crystals (AB_2-like diborides) are $C_{11}>0$, $C_{11}-C_{12}<0$, $C_{44}>0$ and $C_{11}+C_{12}+C_{33}-2(C_{13})^2>0$. Further, different values of elastic compliances of TM diborides are listed in table 1.3 suggesting the anisotropy in distribution of force in different crystallographic directions.

Table 1.3: Elastic compliances corresponding to different TMDBs.

Compound	C_{11}	C_{12}	C_{13}	C_{33}	C_{44}
TiB_2	670.9	64.0	100.9	472.9	266.6
ZrB_2	540.0	55.9	509.0	431.0	250.0
HfB_2	577.0	93.0	129.0	448.0	253.0
VB_2	676.0	115.0	130.0	471.0	238.0
NbB_2	601.0	107.0	185.0	439.0	220.0
TaB_2	498.1	195.0	232.0	434.9	145.6
CrB_2	583.1	177.9	187.2	371.8	154.4
MoB_2	618.0	130.0	206.0	432.3	168.9
WB_2	632.5	140.8	241.6	426.2	133.3

Moreover, Voigt–Reuss–Hill [14] derived a mathematical dependency of bulk modulus (K), shear modulus (G), Young's modulus (E), and Poisson's ratio (σ) on various elastic compliances for simple hexagonal crystal structure which are as follows;

$$B_{Voigt} = \frac{2}{9}\left(C_{11} + C_{12} + \frac{C_{33}}{2} + 2C_{13}\right) \tag{1.1}$$

$$G_{Voigt} = \frac{1}{30}(7C_{11} - 5C_{12} + 12C_{44} + 2C_{33} - 4C_{13}) \tag{1.2}$$

$$B_{Reuss} = \frac{(C_{11} + C_{12})C_{33} - 2C_{13}^2}{C_{11} + C_{12} + 2C_{33} - 4C_{13}} \tag{1.3}$$

$$G_{Reuss} = \frac{5}{2}\left\{\frac{[(C_{11} + C_{12})C_{33} - 2C_{13}^2]C_{44}\left(\frac{C_{11} - C_{12}}{2}\right)}{3B_V C_{44}\left(\frac{C_{11} - C_{12}}{2}\right) + [(C_{11} + C_{12})C_{33} - 2C_{13}^2]\left(C_{44} + \frac{C_{11} - C_{12}}{2}\right)}\right\} \tag{1.4}$$

$$B_{Hill} = \frac{(B_V + B_R)}{2};\ G_{Hill} = \frac{(G_V + G_R)}{2};\ E = \frac{9BG}{(3B + G)} \tag{1.5}$$

$$\nu = \frac{(3B - 2G)}{[2(3B + G)]} \tag{1.6}$$

As we move down in group IV-VI, there is no specific trend in the variation of shear modulus (G) and elastic modulus (E) but, the deviation of the magnitudes of moduli is narrow in a particular group and different values of elastic constants are enlisted in table 1.4. The Poisson's ratio (ν) is also small which is due to strong covalent bonding [16].

Table 1.4: Various elastic properties of transition metal diborides.

Compound	Bulk modulus, B (GPa)	Elastic modulus, E (GPa)	Shear modulus, G (GPa)	Poisson ratio (ν)	B/G
TiB_2	240.0	551.0	225.0	0.11	1.06
ZrB_2	248.0	500.0	220.0	0.18	1.12
HfB_2	232.0	480.0	243.0	0.12	0.95
VB_2	279.5	562.2	240.9	0.16	1.16
NbB_2	286.3	507.0	210.4	0.20	1.36
TaB_2	305.4	551.0	138.7	0.32	2.20
CrB_2	287.6	409.6	164.4	0.28	1.75
MoB_2	304.4	463.1	186.0	0.24	1.63
WB_2	348.0	469.0	164.1	0.29	2.12

1.4.2. Microhardness

Hardness depends on the elasticity and plasticity of a material and tells how resistive a material is to scratch and wear. Which is characterized by indentation. Group IV diboride possess better resistance to these mechanisms than those of groups V and VI which results to their higher hardness and better stability.

Table 1.5: Various hardnesses of transition metal diborides.

Compound	Hardness (GPa)	Compound	Hardness (GPa)	Compound	Hardness (GPa)
TiB_2	25.5	VB_2	26.5	CrB_2	16.0
ZrB_2	17.9	NbB_2	20.9	MoB_2	15.2
HfB_2	24.0	TaB_2	25.6	WB_2	26.0

1.4.3. Ductility and brittleness

Ductility and brittleness of AB_2 type structure is described by Cauchy pressure and the ratio of bulk modulus to shear modulus (B/G) as listed in table 1.4. Petti explained that cauchy pressure is positive for a ductile material, while it's negative if material is brittle [17]. The Cauchy pressures for simple hexagonal crystals increases with increasing valence electrons concentration [18]. Pugh proposed B/G ratio to identify that if $\frac{B}{G} < 1.75$, a material is brittle; or $\frac{B}{G} > 1.75$ material is ductile [19]. Poisson's ratio plays an important role as $\nu < 0.26$, material is ductile and $\nu < 0.26$, material is brittle [20]. B/G ratios of various TM diborides are enlisted in table 1.4 from which CrB_2, TaB_2 and WB_2 have $\frac{B}{G} > 1.75$ suggesting their higher brittleness as compared to other TM diborides.

1.5. Chemical stability

As TMBs have high melting points so, they have high chemical stability [21]. In the periodic table, atomic radius increases going from left to right form group IV to group VI, as a consequence of temperature of this melting TMBs decreases. In the case of transition metals the number of bonding states increases with the increase in number of d electrons and reaches a maxima in the middle of the series [7]. A comparison between the diborides of IV-A and V-A group metals has shown that NbB_2 has the highest chemical stability because of its strong bonding between B–B and Nb–B than other diborides [22].

1.6 Application of TMDBs

Boron is used in fission reaction to absorb neutron due to which it can be used in fast breeder reactors for overcoming the world energy shortages [1]. Kislyi and Samsonov used borides in

the form of thermocouple material. ZrB_2 is used in nuclear energy plants in the form of control rods. Titanium diboride (TiB_2) has been used as a crucible material for melting the non-ferrous metals as it does not react with molten copper, zinc or aluminium [23]. Hough used TiB_2 for preparation of fibers in composite materials [24]. Meibuhr used Nickel boride (NiB) as a catalyst in organic chemistry and in fuel cells [25]. AB_2 type transition metal diborides have been used as coatings and corrosion resting application in various composites because of their high hardness and good thermal stability.

1.7 Nb-B system

The phase diagram of niobium and boron contains five Nb-B compounds as NbB, Nb_3B_2, Nb_5B_6, Nb_3B_4 and NbB_2 as shown in figure 1.5. In Nb-B system, to obtain a sample within a certain stability range of temperature and composition, it is important to choose right synthesis method. Almost all the TMBs are synthesized at very high temperatures. For example, to synthesize Nb_3B_2, a high temperature of 2050°C is required which causes decomposition of the chosen phase.

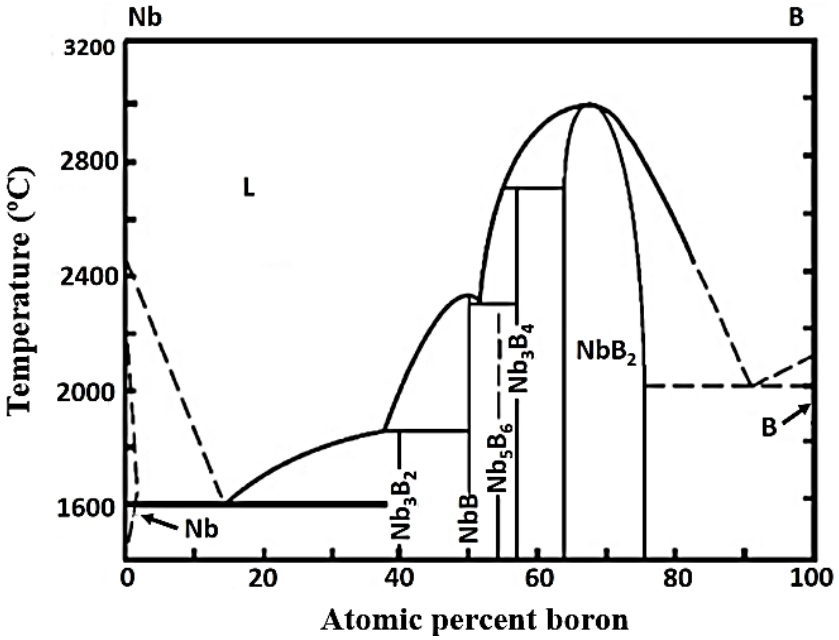

Figure 1.5: Binary phase diagram of the Nb-B system [26].

1.7.1 Niobium diboride (NbB_2)

The structure of diboride can be explained on the basis of a simple chemistry by taking the example of NbB_2, in which Nb atoms are located at (0,0,0) and B atoms at (1/3,2/3,1/2) and (2/3,1/3,1/2) lattice sites, respectively. As it is known that B atoms form a simple hexagonal pattern forming a covalent bond with Nb through which their strength is determined [27]. NbB_2 is a vital compound among all the TMDBs due to its distinctive physical and chemical

properties including high value of melting point (~2900 °C), thermal expansion coefficient of (~8.0 x 10^6 /°C). It has a low density (~6.97 g/cm^3) with ~21 VHN and a bulk modulus of 286 GPa. The B/G ratio of NbB_2 is 1.3 which according to Pugh falls under the category of brittle materials which inturn makes it hard.

1.7.2 Application of Niobium diborides

NbB_2 also falls under the category of refractory materials and have excellent oxidation stabilities at high temperatures [6]. NbB_2 finds application at high temperature because of it low melting metal oxides Nb_2O_5 (1512 °C) and NbO_2 (1915 °C) [28–31]. NbB_2 is used as electrodes for refining of aluminium [32], in hypersonic aerospace vehicles [33], in high speed cutting tools, in refractories for molten metal contact applications, plasma-facing materials for nuclear fusion reactors [34], and fuel forms for advanced nuclear fission reactors [35]. Some of the major utility of NbB_2 in engineering applications are mention as follows;

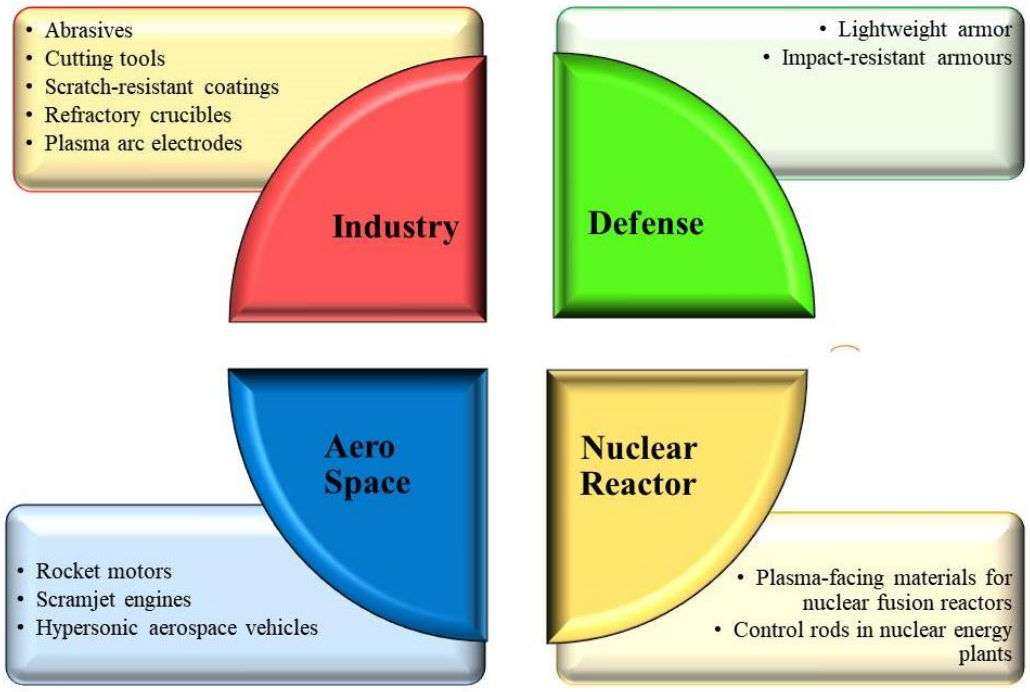

Figure 1.6: Application of niobium diborides in various fields.

References

[1] V. Matkovich, Boron and refractory borides, Springer-Verlag, 1977.

[2] G.B. Raju, B. Basu, Development of high temperature TiB_2-based ceramics, Key Eng. Mater. 395 (2009) 89–124.

[3] W.G. Fahrenholtz, J. Binner, J. Zou, Synthesis of ultra-refractory transition metal diboride compounds, J. Mater. Res. 31 (2016) 1–16.

[4] K.K. Maeda, S.M.H. Maeda, T. Yoshikawa, Synthesis of ultrafine NbB_2 powder by rapid carbothermal reduction in a vertical tubular reactor, J. Alloys Compd. 215 (1994) 127–134.

[5] W. Hayami, A. Momozawa, S. Otani, Effect of defects in the formation of AlB_2-Type WB_2 and MoB_2, Inorg. Chem. 52 (2013) 7573–7577.

[6] N.I. Medvedeva, A.L. Ivanovskii, J.E. Medvedeva, A.J. Freeman, Electronic structure of superconducting MgB_2 and related binary and ternary borides, 64 (2001) 1–4.

[7] P. Vajeeston, P. Ravindran, C. Ravi, R. Asokamani, Electronic structure , bonding , and ground-state properties of AlB_2 -type transition-metal diborides, Phys. Rev. B. 63 (2001) 1–12..

[8] P. De, M. Castro, G. Tavizón, Comparative study of the electronic structure of alkaline-earth borides (MeB_2; Me = Mg , Al , Zr , Nb , and Ta) and their normal-state conductivity. 169 (2002) 168-175

[9] B. Post, F.W. Glaser, D. Moskowitz, Transition metal diborides, Acta Metall. 2 (1954) 20–25.

[10] Z. Zachariev, New superhard ternary borides in composite materials, in: Met. Ceram. Polym. Compos. Var. Uses, Bulgaria 2005.

[11] Standard test method for linear thermal expansion of solid materials with a push-rod dilatometer, in: ASTM Int. (2011) 1–9.

[12] B. Lönnberg, Thermal expansion studies on the group IV-VII transition metal diborides, J. Less-Common Met. 141 (1988) 145–156.

[13] J. Castaing, R. Caudron, G. Toupance, P. Costa, Electronic structure of transition metal diborides, Solid State Commun. 7 (1969) 1453–1456.

[14] R. Hill, The elastic behaviour of a crystalline aggregate, Proc. Phys. Soc. 65 (1952) 349–354.

[15] C. Kittel, Introduction to Solid State Physics, Wiley (1996).

[16] C. Qi, Y. Jiang, Y. Liu, R. Zhou, Elastic and electronic properties of XB_2 (X=V, Nb, Ta, Cr, Mo, and W) with AlB_2 structure from first principles calculations, Ceram. Int. 40 (2014) 5843–5851.

[17] A.L. Ivanovskii, Mechanical and electronic properties of diborides of transition 3d-5d metals from first principles: Toward search of novel ultra-incompressible and superhard materials, Prog. Mater. Sci. 57 (2012) 184–228.

[18] D.G. Pettifor, Theoretical predictions of structure and related properties of intermetallics, Mater. Sci. Technol. 8 (1992) 345–349.

[19] S.F. Pugh, XCII. Relations between the elastic moduli and the plastic properties of

polycrystalline pure metals, in: London, Edinburgh, Dublin Philos. Mag. J. Sci. 45 (1954) 823–843.

[20] M.C. Gao, Ö.N. Doğan, P. King, A.D. Rollett, M. Widom, The first-principles design of ductile refractory alloys, Jom. 60 (2008) 61–65.

[21] P. Vajeeston, P. Ravindran, C. Ravi, R. Asokamani, Electronic structure, bonding, and ground-state properties of AlB_2-type transition-metal diborides, Phys. Rev. B. 63 (2001) 45115.

[22] A.L. Ivanovsky, N.I. Medvedeva, J.E. Medvedeva, Quantum-chemical analysis of the chemical stability and cohesive properties of, Mendeleev Commun. 8 (1998) 129–131.

[23] A.W. Weimer, Carbide, Nitride and Boride materials synthesis and processing, chapman and hall. 1997.

[24] R.L. Hough, W. Air, F. Base, Pyrolytic Titanium Diboride Filaments for Composites, AIAA J. 4 (1966) 107–111.

[25] S.G. Meibuhr, Nickel boride hydrogen anodes, Electrochim. Acta. 12 (1967) 1059–1063.

[26] A. Gubernat, Pressureless sintering of single-phase tantalum carbide and niobium carbide, J. Eur. Ceram. Soc. 33 (2013) 2391–2398.

[27] J.J. Gilman, Chemistry and Physics of Mechanical Hardness, wiley 2009.

[28] M.L. Bauccio, Selection of structural material, in: ASM Int. Mater. Park, 1994.

[29] W.G. Fahrenholtz, G.E. Hilmas, I.G. Talmy, J.A. Zaykoski, Refractory diborides of zirconium and hafnium, J. Am. Ceram. Soc. 90 (2007) 1347–1364.

[30] R.G. Munro, Material properties of titanium diboride, J. Res. Natl. Inst. Stand. Technol. 105 (2000) 709-720.

[31] X. Zhang, G.E. Hilmas, W.G. Fahrenholtz, Synthesis, densification, and mechanical properties of TaB_2, Mater. Lett. 62 (2008) 4251–4253.

[32] E. Wuchina, M. Opeka, S. Causey, K. Buesking, J. Spain, A. Cull, J. Routbort, F. Guitierrez-Mora, Designing for ultrahigh-temperature applications: The mechanical and thermal properties of HfB_2, HfC_x, HfN_x and αHf(N), J. Mater. Sci. 39 (2004) 5939–5949.

[33] D.M. Van Wie, D.G. Drewry, D.E. King, C.M. Hudson, The hypersonic environment: Required operating conditions and design challenges, J. Mater. Sci. 39 (2004) 5915–5924.

[34] T.A. Jackson, D.R. Eklund, A.J. Fink, High speed propulsion: Performance advantage of advanced materials, J. Mater. Sci. 39 (2004) 5905–5913.

[35] K. ichi Takagi, Development and application of high strength ternary boride base cermets, J. Solid State Chem. 179 (2006) 2809–2818.

2. Literature Review

Transition metal diborides (TMBs) have been introduced in the previous chapter along with their various characteristics and properties. Diborides are being synthesised by scientists all around the world among which H. Moissan identified a number of diboride compounds in 19th century. G. F. Tavadze, Alexander, S. Shteinberg, V. Matkovich categorized TM diborides as per their different properties. Among all TMBs, niobium diboride (NbB_2) attains an essential importance as an industrial material. Some of the latest developments on NbB_2 are summarized in this chapter which are as follows:

In 1975**, Motojima *et al.*** [1] synthesized niobium diboride (NbB_2) by chemical vapour deposition technique in which a gaseous mixture of $NbCl_5$, BCI_3, H_2 and Ar was heated to 950-1200 °C. They observed the formation of a homogeneous film created at 950 to 1050 °C, pillar crystals at 1050 to 1200 °C and NbB_2 to react with the quartz above 1200 °C to attain Nb_5Si_3.

In 1989, **Matsudaira *et al*.** [2] prepared niobium boride powders through solid state reaction of niobium metal powder and amorphous boron powder. They suggested that the formation of niobium boride is a function of synthesis temperature which was asserted by the formation of ($NbB+NbB_2$) at 1000 ^oC followed by the formation of Nb_3B_4 at much higher temperature i.e. 1800 ^oC. Moreover, heating up to 1600 ^oC (intermediate temperature) for 15 min holding resulted to single phase NbB_2 in Ar atmosphere to avoid oxidation of synthesized products. In the same sequence**, Maeda *et al*.** [3] used carbothermal reduction route to get the NbB_2 powder. In the multi-step synthesis process, the reduced mixture of Nb_2O_5, B_2O_3 and C was obtained from the heating of Nb_2O_5, H_3BO_3 and corn starch. Hereafter, the mixture was placed downwards in the presence of Ar atmosphere in the vertical tubular reactor to obtain NbB_2. They observed that formation of NbB_2 depends on the ignition temperature of the herald, herald dimensions and temperature of the process used. The carbonaceous material in the herald particles was less volatile when corn starch was ignited at 400 °C as compared to 700 °C. For optimized production of NbB_2, the smaller herald dimensions and the longer the herald particles might stay in the reaction zone is required. Under optimum conditions, the NbB_2 crystallites were as small as 40-50 nm and the residual carbon content was 2.65 % by mass**.**

In 2002**, Yamamoto *et al*.** [4] synthesized $Nb_{1-x}B_2$ under high pressure to examine the crystal structure and superconductivity. At 5 GPa pressure superconductivity of synthesized NbB_2 was observed at transition temperature (T_c) above 9 K. But below 3 K, no clear

superconductivity was observed. It was recommended that the amount of band overlap is a crucial parameter to control T_c due to the variation in lattice parameter associated to Nb deficiency in $Nb_{1-x}B_2$. Further, the sintering at 1200 ^oC resulted to more Nb deficient system having higher T_c.

In 2005**, Peijun *et al***. [5] prepared niobium diboride (NbB_2) nano rods in the autoclave by reacting of $NbCl_5$ with $NaBH_4$ in the temperature range of 550–650 ^oC.

$$NbCl_5 + NaBH_4 \rightarrow NbB_2 + NaCl + H_2 \quad (2.1)$$

It was verified by the X-ray diffraction (XRD). By the transmission electron diffraction of synthesized sample measured average diameter is 50-60 nm rods length is 600nm.

In 2006**, Tsuchida *et al.*** [6] have taken Nb:B:C=2:2:1 mloar ratio to synthesized of NbC and NbB_2 mixture through mechanical activated (MA) by ball milling for 105 min. The powder was promote become self ignited and self propagating high temperature synthesis (SHS) [7]. Further they prepared pellet of synthesized powder with or without MA-SHS and perform spark plasma sintering at 1800 ^oC for 10 min. They concluded that hardness of MA-SHS sintered pellet was 19.8 GPa and without MA-SHS hardness of pellet was 16.6 GPa.

Kiyokata *et al*. [8] synthesized NbB_2 by mechano-chemical route in which a mixture of powder Nb-B (1:2) was milled in a planetary ball mill at 600 rpm for different durations (5, 10, 20, and 50 h) and with different diameter balls (5, 9 and 16 mm). When the mixture was milled with 5 mm diameter balls, NbB_2 started to form in 20 h and the single phase NbB_2 was obtained in 50 h. They concluded that if ball diameter increases then the time required to obtain NbB_2 phase and single phase is reduced which is enlisted as follows table 2.1:

Table 2.1: Relation between size of balls and time required for synthesized of the NbB_2.

Ball diameter (mm)	**Time required to start the formation of NbB_2 (h)**	**Time required to obtain single phase NbB_2 (h)**
5	20	50
9	10	30
16	5	20

The particle size of synthesized powder was measured by light scattering instrument and crystallite size was measured by X-ray line broadening method is given below in table 2.2 which indicates high degree of agglomeration of nano particles.

Table 2.2: Average particle size and crystallite size of so obtained NbB_2 powder at 50 h milling.

Ball diameter (mm)	Average particle size (mm)	Crystallite size (nm)
5	370	6.1
9	370	6.2
16	980	5.9

In the same year **Yeh *at el.***[9] used self-propagating high-temperature synthesis (SHS) to synthesize niobium borides such as Nb_3B_2, NbB, Nb_5B_6, Nb_3B_4, and NbB_2. They had blended the sample through ball milling for 10 h of preheated Nb and B at 200-300 ^oC by taking the different ratio of Nb and B as 3:2, 1:1, 5:6, 3:4, and 1:2. They studied the effects of preheating temperature and starting stoichiometry on combustion characteristics of the product composition. They verified by XRD that phase had not been transformed completely in the ratio of 3:2, 5:6 and 3:4 in which major amount of Nb and Nb_3B_4 left and in 1:1, 1:2 NbB and NbB_2 phase obtained respectively and neglected the small amount of Nb and Nb_3B_4. **Yeh *et al.*** [10] synthesized NbB and NbB_2 by self-propagating high-temperature synthesis (SHS). They studied the effect of preheating temperature. Before the ignition, the compacted powder was heated at 200 and 300 ^oC, which was made up of 1 Nb and 1 B by the SHS reaction and through this Nb_3B_4 was formed in small amount, but further Nb and B ratio was taken to 1:2, so to optimize NbB_2. They suggested that preheating temperature and sample density did not affect final composition of products but affected the dynamics of the combustion wave. The initial reactant ratio was taken more precise by to optimize boride phase in the final product. By increasing the preheating temperature, they observed that, the rate of combustion wave increased with combustion temperature. Synthesis of NbB and NbB_2 was found to be dependent on the temperature of combustion wave velocity. The optimized product (NbB and NbB_2) with other boride phase (Nb_3B_4) was synthesized from the niobium boride which was identified through XRD technique.

In 2008**, Ma *et al.*** [11] synthesized NbB_2 through the inorganic-solvent-thermal route by the mixing of molten salt (prepared by NaCl and $MgCl_2$ in glove box under N_2 atmosphere), metallic Mg, Nb_2O_5 and boric acid in autoclave at 650 ^oC under Ar atmosphere. They identified the optimized phase by the XRD powder technique and particles size of NbB_2 was 30 nm verified by scanning electron microscopy. They observed the thermal stability of synthesized NbB_2 nanoparticle by TGA and concluded that below 500 ^oC NbB_2 have good thermal stability and oxidation resistance in the air atmosphere.

In 2014, **Sairam *et al.*** [12] optimized the synthesis condition of NbB_2 by performing heat treatment of Nb and B in two stages. Preliminary, they had synthesized NbB_2 at 1200 °C with the holding time of 1 min and 15 min under load and no load conditions, respectively. Further heat treatment at 1700 °C to 1900 °C for 15 min under load of 12.5 KN by spark plasma sintering (SPS) technique had been done in which the density of sintered NbB_2 was increased at 1900 ^oC. They measured the micro-hardness of NbB_2 i.e 20.25±1.75 GPa. Hardness was reduced with the increased indentation load and extended a saturation of 16.5±0.6 GPa corresponding to 5 Kg load. Elastic modulus 539±5 GPa and fracture toughness 4.0±0.6 MPa. $m^{1/2}$ of sintered NbB_2.

In 2014, **Demirskyi *et al.*** [13] synthesized and sintered $B_4C–NbB_2$ eutectic composite through the modern method of SPS by the adjusting pressure. They planned a route of *in situ* formation of strengthened eutectic composites, consisting of a matrix B_4C and $B_4C–NbB_2$ composite by changing the pressure, temperature and composition and also containing regularly distributed whiskers of NbB_2. They optimized high hardness of these eutectic composition. The vickers hardness of the prepared samples was 25–26 GPa for B_4C matrix and 26–30 GPa for $NbB_2–B_4C$ eutectic grains. 60 mol% NbB_2 composites had fracture toughness of 7.2-1.2 MPa.$m^{1/2}$.

In 2015, **Yeh *et al***. [14] adopted self-propagating high-temperature synthesis (SHS) procedure to synthesize the NbB_2 and mullite ($Al_2O_3–SiO_2$ system) composites by using a mixture of Nb_2O_5, B_2O_3, Al and Si in molar ratio which is given as follows;

(A)	$\frac{13}{11}Nb_2O_5 + \frac{26}{11}B_2O_3 + 6Al + xSi$	x = 2.0-3.0
(B)	$\frac{13}{9}Nb_2O_5 + \frac{52}{27}B_2O_3 + \frac{52}{27}B + 6Al + ySi$	y = 2.0-3.0

They added more boron in composition (B) to increase the NbB_2 yield. They studied the combustion performance and phase transformation due to *in-situ* formation of SiO_2 as shown in the following reaction:

$$\frac{6}{5}Nb_2O_5 + B_2O_3 + \frac{14}{5}B + 6Al + 2SiO_2 \rightarrow \frac{12}{5}NbB_2 + (3Al_2O_3.2SiO_2) \quad (2.2)$$

They compared Si sample with the combustion of the SiO_2 accepted sample. Former showed more exothermic and active by the drop of B_2O_3 because of additional Si metallothermic reduction of B_2O3 was significantly enhanced. NbB_2 and mullite composite was obtained.

They added SiO_2 due to lack of B_2O_3, then the product became consisted of mullite and three boride phases NbB, Nb_3B_4, and NbB_2 and an amorphous compound. After the additives of Al and Si, the reaction became more exothermic combustion, higher self-sustainability, shorter reaction time and better phase transformation.

Balci *et al*. [15] synthesized NbB_2-NbC composite powder through the carbothermal route by ball milling for different timing (0,1,3 and 5 h) by taken stoichiometric amount of Nb_2O_5, B_2O_3 and C. Further, they annealed blended powder at 1300 ^oC-1400 ^oC. They concluded through XRD analysis of synthesized powder, NbB_2 phase increases and NbC phase decreases with increases milling time and increases anneling temperature. The maximum amount of NbB_2 phase obtained by the 5 h milling and 12 h anneling at 1400 ^oC. The details of optimization of NbB_2-NbC composite is given as follows:

Table 2.3: Quantitative phase analyses of blended powder milled and annealed at (0, 1, 3 and 5 h) and (1300 and 1400 ^oC) respectively.

Milling time (h)	**Annealing temperature (^oC)**	**NbB_2 (wt %)**	**NbC (wt %)**	**Nb_3B_4 (wt %)**	**C (wt %)**
0	1300	-	92.9	-	7.1
1		49.1	40.1	6.2	4.6
3		82.3	14.5	3.2	-
5		87.5	8.1	4.4	-
0	1400	25.6	70.4	-	4.0
1		67.9	30.0	-	2.1
3		89.7	10.3	-	-
5		98.0	2.0	-	-

Jafari *et al*. [16] synthesized NbB_2 by the reaction of Al and Mg to B_2O_3 with Nb through the mechanochemical process. They identified the phase and structure by X-ray diffractometry, scanning electron microscopy (SEM), transmission electron microscopy (TEM). They observed the formation of $AlNb_2$ due to aluminothermic reaction, NbB_2 due to magnesiothermic reduction and $Mg_3(BO_3)_2$ as major phase by mechanically induced self-sustaining reaction (MSR) milling for 2.4 hr. $AlNb_2$, $Mg_3(BO_3)_2$ got removed as the milling duration was increased to 5 h and reoccurrence was observed after 40 h milling which confirms the reversibility of synthesis path.

Torabi *et al.* [17] used the Mg, B_2O_3, Nb and C in mechano-chemical method to synthesized NbB_2 and NbC composite. They indicated through thermal analysis, the reduction and synthesis reactions were highly exothermic and should be self-sustaining. They studied the differential thermal analysis (DTA) followed the different reaction paths without changing the reaction temperature. They eliminated Mg step by step by using mechanical working. After 2h mechanical working through the expanded the MSR reaction, NbB_2 phase had been with the absence of NbC phase.

In 2016**, Balcı *et al.*** [18] studied the effect of sintering techniques on the microstructure and mechanical properties such as hardness, wear volume, elastic modules and fracture toughness. Primarily, they synthesized the mixture of niobium borides (NbB, Nb_3B_4, and NbB_2) from Nb_2O_5, $B_2O_3$and Mg by the mechano-chemical process. After that, they prepared the pellets of as synthesized mixture with or with-out the additives. The amount of additives (cobalt, Co) was taken as 2% and 5%. As prepared pellets were sintered via cold pressing/pressure-less and SPS. The cold pressing/pressure less sintering was done under inert atmosphere (Ar) at 1500 ^oC for 4 h in a LinnTM HT-1800 high-temperature controlled-atmosphere furnace. SPS (without additives) was done for 15 min at 1500 ^oC under the holding pressure of 60 MPa. Micro-hardness of 24–28 GPa, wear volume loss of 2.8–4.5 × 10^{-4} mm^3, elastic modulus of 508–552 GPa and fracture toughness of 4.05–4.74 MPa was obtained. The relative density of SPS sintered sample was 83.75%. Micro hardness of 13.68 MPa wear volume loss of 11.5× 10^{-4} mm^3 and elastic modules was 243 GPa, fracture toughness of 2.07 MPa was obtained in SPS sintered sample. They suggested that, increasing the quantity of Co, the micro hardness has increased with small decrement in relative wear resistance and toughness in pressure less sintering as enlisted as follows:

Table 2.4: Wear volume loss, relative wear resistance, hardness, elastic modulus, fracture toughness values of the sintered niobium borides.

Sample	**Wear Volume Loss (×10^{-4} mm^3)**	**Relative Wear Resistance**	**$HV_{0.2}$ (GPa)**	**Elastic Modulus (GPa)**	**Fracture Toughness ($MPa.m^{1/2}$)**
N5-PS	125.0	1.0	1.92 ± 0.31	88.7	-
N5-2CoPS	2.8	44.6	24.82 ± 0.06	552.2	4.05 ± 0.64
N5-5CoPS	4.5	27.8	27.17 ± 0.85	508.8	4.74 ± 0.23
N5-SPS	11.5	10.9	13.68 ± 0.73	243.0	2.07 ± 0.08

Balcı *et al*. [19] used powder metallurgy method to obtain NbB, NbB_2, and Nb_3B_4. They blended Nb_2O_5, B_2O_3 and Mg via ball milling for the different time at room temperature. They optimized the synthesis parameters to obtain single phase NbB_2. A mixture of NbB, NbB_2, and Nb_3B_4 was obtained after 2 h milling which got transformed to single phase NbB_2 at 5 h milling. After that, removal of MgO phase was done through leaching. After that, annealing at 1500 ^oC for 4 h a mixture of NbB and NbB_2, Nb_3B_4 phase completely transfer in to NbB.

Demirskyia *et al*. [20] synthesized SiC–NbB_2 eutectic composites by spark plasma sintering (SPS) at 1950– 2100 °C via the *in situ* formation of eutectic grains during consolidation. They measured micro hardness at an indentation load of 9.8 N and toughness of sintered composites, which were comparable with earlier finding for SiC–TiB_2 and SiC–ZrB_2 eutectics [21,22]. They reported the temperature dependence of the flexural strength of the SiC–NbB_2 system. Ceramic composites with eutectic structure exhibited an unchanged strength of 400-600 MPa and an elastic modulus of 430 ± 30 GPa at room temperature and at 1600 °C. Further they concluded that increase in testing temperature up to 1900 °C, strength was slight by decreased and this behaviour was attributed to the increase in plastic deformation at the time of fracture process.

References

[1] S. Motojima, K. Sugiyama, Y. Takahashi, Chemical vapour deposition of niobium diboride (NbB_2), J. Cryst. Growth. 30 (1975) 233–239.

[2] T. Matsudaira, H. Itoh and S. Naka, Synthesis of niobium boride powder by solid state reaction between niobium and amorphous boron, J. Less-Common Met. 155 (1989) 207–214.

[3] H. Maeda, T. Yoshikawa, K. Kusakabe, S. Morooka, Synthesis of ultrafine NbB_2 powder by rapid carbothermal reduction in a vertical tubular reactor, J. Alloys Compd. 215 (1994) 127–134.

[4] A. Yamamoto , C. Takao, T. Masui, M. Izumi, S. Tajima, High-pressure synthesis of superconducting $Nb_{1-x}B_2$ (x= 0–0.48) with the maximum T_c = 9.2K, 383 (2002) 197–206.

[5] P. Cai, Z. Yang, L. Shi, L. Chen, A. Zhao, Y. Gu, Y. Qian, Low temperature synthesis of NbB_2 nanorods by a solid-state reaction route, Mater. Lett. 59 (2005) 3550–3552.

[6] T. Tsuchida, T. Kakuta, Fabrication of SPS compacts from NbC–NbB_2 powder mixtures synthesized by the MA–SHS in air process, J. Alloys Compd. 415 (2006) 156–161.

[7] T. Tsuchida, T. Hasegawa, M. Inagaki, Self-Combustion Reactions Induced by Mechanical Activation: Formation of Aluminum Nitride from Aluminum-Graphite Powder Mixture, J. Am. Ceram. Soc. 2 (1994) 3227–3231.

[8] K. Iizumia, C. Sekiyab, S. Okadac, K. Kudoud, T. Shishido, Mechanochemically assisted preparation of NbB_2 powder, J. Eur. Ceram. Soc. 26 (2006) 635–638.

[9] C.L. Yeh, W.H. Chen, A comparative study on combustion synthesis of Nb–B compounds, J. Alloys Compd. 422 (2006) 78–85.

[10] C.L.Yeh, W.H. Chen, Preparation of niobium borides NbB and NbB_2 by self-propagating combustion synthesis, J. Alloys Compd. 420 (2006) 111–116.

[11] J. Ma, Y. Duc, M. Wu, G. Li, Z. Feng, M. Guo, Y. Sun, W. Song, M. Lin, X. Guo, A simple inorganic-solvent-thermal route to nanocrystalline niobium diboride, J. Alloys Compd. 468 (2009) 473–476.

[12] K. Sairam, J.K. Sonber, T.S.R. Ch. Murthy, C. Subramanian, R.K. Fotedar, R.C. Hubli, Reaction spark plasma sintering of niobium diboride, Int. J. Refract. Met. Hard Mater. 43 (2014) 259–262.

[13] D. Demirskyi, Y. Sakka., *In-situ* fabrication of B_4C-NbB_2 eutectic composites by spark-plasma sintering, J. Am. Ceram. Soc. 97 (2014) 2376–2378.

[14] C.L. Yeh, C.C. Chou, Formation of NbB_2/mullite composites by combustion synthesis involving metallothermic reduction of Nb_2O_5 and B_2O_3, Ceram. Int. 41 (2015) 14592–14596.

[15] Ö. Balcı, D. Ağaoğulları, D. Ovalı, L. Öveçog ˘lu, İ. Duman, In situ synthesis of NbB_2–NbC composite powders by milling-assisted carbothermal reduction of oxide raw materials Özge, 26 (2015) 1–10.

[16] M. Jafari, H. Tajizadegan, M.H. Golabgir, A. Chami, O. Torabi, Investigation on mechanochemical behavior of Al/Mg-B_2O_3-Nb system reactive mixtures to synthesize niobium diboride, Int. J. Refract. Met. Hard Mater. 50 (2015) 86–92.

[17] O. Torabin, S. Naghibi, M.H. Golabgira, H. Tajizadegana, A. Jamshidia, Mechanochemical synthesis of NbC-NbB2 nanocomposite from the Mg/B_2O_3/Nb/C powder mixtures, Ceram. Int. 41 (2015) 5362–5369.

[18] Ö. Balcı, D. Ağaoğulları, F. Muhaffel, M.L. Övec¸o˘glu, H. C¸imeno˘glu, İ. Duman, Effect of sintering techniques on the microstructure and mechanical properties of niobium borides, J. Eur. Ceram. Soc. 36 (2016) 3113–3123.

[19] Ö. Balcı, D. Ağaoğulları, M.L. Öveçoğlu, İ. Duman, Synthesis of niobium borides by powder metallurgy methods using Nb_2O_5, B_2O_3 and Mg blends, Trans. Nonferrous Met. Soc. China. 26 (2016) 747–758.

[20] D. Demirskyi, O. Vasylkiv, Mechanical properties of SiC-NbB_2 eutectic composites by in situ spark plasma sintering, Ceram. Int. 42 (2016) 0–1.

[21] W.J. Li, R. Tu, T. Goto, Preparation of TiB_2 – SiC eutectic composite by an arc-melted method and its characterization, Mater. Trans. 46 (2005) 2504–2508.

[22] R. Tu, H. Hirayama, T. Goto, Preparation of ZrB_2 –SiC composites by arc melting and their properties, J. Ceram. Soc. Japan. 116 (2008) 431–435.

3. Experimental work

On the basis of reviewed literature (discussed in chapter 2) a methodology has been proposed to synthesis NbB_2 nano particles at low temperature. The details of experimental procedures followed in given below:

3.1 Material used

Niobium pentaoxide (Nb_2O_5, *Sigma-Aldrich, 99.99%*) as niobium source, borax ($Na_2B_4O_7 \cdot 10H_2O$) as boron source and Magnesium metal powder (SDFC Ltd) as reducing agent.

$$Nb_2O_5 + 11Mg + Na_2B_4O_7 \rightarrow Na_2O + 11MgO + 2NbB_2 \quad (3.1)$$

3.2 Methodology

To synthesize the NbB_2, powders of (Nb_2O_5) 1.329gm, ($Na_2B_4O_7 \cdot 10H_2O$) 2 gm and (Mg) (2, 2.5 and 3.5 g) were first blended and than transferred in high pressure cylindrical stainless steel autoclave. The autoclave was heated at different temperature, for different duration followed by furnace cooling. The details of the synthesis conditions are enlisted in table 3.1. figure 3.1 shows the methodology followed during the process.

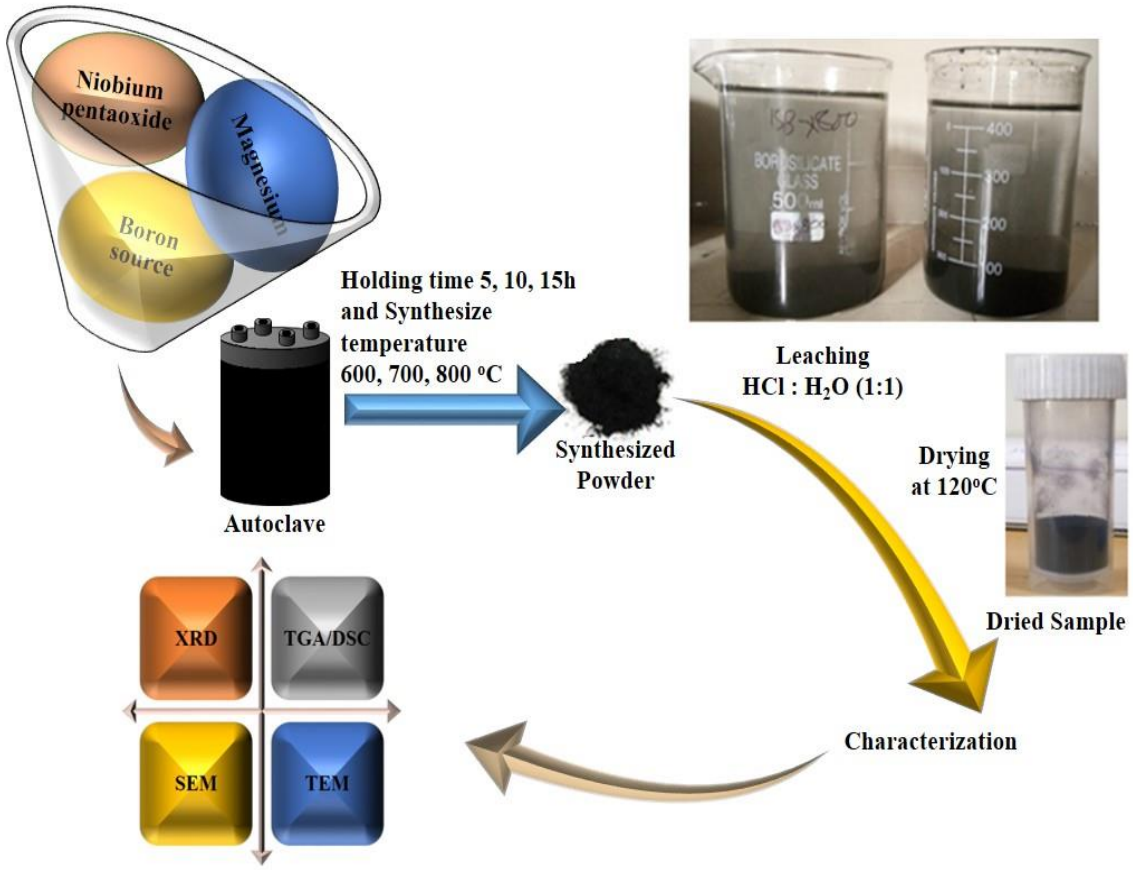

Figure 3.1: Methodology used to synthesize and characterize the Niobium diboride (NbB_2).

Table 3.1: Details of synthesis conditions of NbB_2 nanopowders.

Sample Id	Mg (gm)	Temperature (^oC)	Holding Time (h)
S-1	2.0	600	5
S-2	2.0	600	10
S-3	2.0	600	15
S-4	2.0	700	5
S-5	2.0	700	10
S-6	2.0	700	15
S-7	2.0	800	5
S-8	2.0	800	10
S-9	2.0	800	15
S-10	2.5	600	10
S-11	2.5	600	15
S-12	2.5	700	10
S-13	2.5	700	15
S-14	2.5	800	10
S-15	2.5	800	15
S-16	3.5	600	10
S-17	3.5	600	15
S-18	3.5	700	5
S-19	3.5	700	10
S-20	3.5	700	15
S-21	3.5	800	5
S-22	3.5	800	10
S-23	3.5	800	15

The synthesized powder was taken out from autoclave. The powder was than subjected to loding.Leaching of sample was done by taking HCl:H_2O (1:1) to remove the undesired MgO, B_2O_3, Na_2O and other impurities. Sample was then washed with distilled water for neutralization. The sample was then placed in oven at 120 ^oC for 24 h.

3.3. Characterizations

3.3.1. X-ray diffraction (XRD)

XRD is a Non-destructive analytical techniques, used to get information about the crystallographic structure, chemical composition and physical properties of materials. For this sample is placed in a stainless steel circular holder to ensure homogeneity.

X-rays have the wavelength of the order of few angstroms, which is comparable to the interatomic distance of a crystal. Therefore, X-rays can be diffracted from atoms situated at their respective lattice sites. In 1912, W. L. Bragg designed a relationship between inter-planar distance (d), wavelength of incident X-ray (λ), diffraction angle (θ) and order of the diffraction (n ~1). These relation is called Bragg's law as described below;

$$2d.\sin\theta = n\lambda \quad (3.2)$$

These techniques help in confirming weather synthesized powder is crystalline, mono crystalline or amorphous. XRD analysis of as synthesized samples were done in X'pert Panalytical Pro instrument with Cu-Kα, λ= 0.15406 nm. All samples were scanned in the 2θ range of 20^o-80^o with step size of 0.0131^o degrees at room temperature.

3.3.2. Differential Scanning Calorimetry (DSC)/Thermal Gravimetric Analysis (TGA)

DSC/TGA is a thermal analysis technique to understand thermal properties of materials. This technique gives information about the phase transformation, behavior of the sample and tells about change in weight with variation in temperature.

The apparatus consists of a sample chamber in which material starts changing its physical nature on varying temperature, which results in the oxidation or reduction of material via releasing or absorbing heat respectively. Weight gain or weight loss of sample is due to oxidation or reduction. The weight gain or loss of sample is measured by cantilever beam with respect to the reference material which is stable at operational range of temperature and TGA is referred to measure with respect to a temperature change. The spectrum of S-23 was obtained in the temperature range of 30–800 ºC in air atmosphere at 5 ºC/min heating mode using NETZSCHSTA449F3.

3.3.3. Field Emission Scanning Electron Microscopy (FE-SEM)

FESEM is useful tool for analyzing topographical features, surface morphology, phase distribution, compositional differences and orientational order within the crystal. It also tells the presence of surface defects. FE-SEM provides simple imaging system, a very wide magnification range and has excellent depth of field. For FESEM study, the synthesized samples S-23 was suspended in ethanol and ultra-sonication was done to avoid agglomeration of particles. One drop of sample was dropped on carbon-coated copper grid dispersed in ethanol. After this gold coating was applied on the copper grid. Analysis was done with *SIGMA Carl Zeiss* FE-SEM at 20 kV.

3.3.4. Transmission Electron Microscopy (TEM)

This technique is used to study different phases and their crystallographic features by transmitting beam of electron through an ultra-thin specimen. The image formed is then magnified on an imaging apparatus, like a fluorescent screen which is later detected by a sensor or a special kind of camera (CCD). At higher level of magnifications the TEM image provides a bright contrast in images due to absorption of electrons, or due to material's thickness. Whereas at very large magnification, lattice fringes are observed. For sample

preparation, S-23 was suspended in ethanol followed by the deposition of this suspension on carbon coated copper grid and analysis in *JEOL 2100F* at 200kV.

4. Results and discussion

Proposed work aims to efficient production of NbB_2 at nano scale involving low synthesis temperature. The effect of synthesis parameters such as temperature, holding time and amount of reducing agent on the synthesis of NbB_2 have been discussed in this chapter.

4.1 XRD analysis

To study the effect of various reaction parameters, all experiments have been categorized on the basis of amount of reducing agent i.e. Mg into two sections: A) less Mg content (2.0g), B) Moderate Mg content (2.5g) and C) high Mg content (3.5g). All the synthesized samples were characterized by XRD to determine the phases obtained at different synthesis conditions. Phase confirmation was done with the help of ICDD cards in *PANalytical X'Pert High score Plus* tool. The details of the ICDD cards which were used to identify phases are enlisted below.

Table 4.1: Details of ICDD cards used in phase identification.

Compound	Symbol	ICDD card	Compound	Symbol	ICDD card
Nb_2O_5	ϕ	00-027-1003	Nb_3B_4	δ	03-065-2553
Nb_2O_5	Δ	00-028-1312	Nb_5B_6	χ	00-042-1040
NbO_2	ε	01-085-0379	NbB	γ	00-032-0709
NbO_2	η	01-071-0020	NbB_2	β	00-035-0742
NbO_2	α	01-082-1142			
Nb_4O_5	*	01-077-0844			

A. Less Mg content (2.0g)

To synthesize NbB_2 at low temperature, Nb, Mg and B were taken in molar ratio 1:16.5:1. Experiments carried out with 2.0g Mg have been sub-divided according to synthesis temperatures (600, 700 and 800 °C) and is discussed in this section.

Synthesis temperature 600 °C: Figure 4.1 shows the XRD patterns of all the samples S-1, S-2 and S-3 synthesized at 600 ^oC with the holding time of 5, 10 and 15 h respectively. As a result of the holding of 5h at 600 ^oC, S-1 consisted Nb_2O_5, NbO_2 and Nb_4O_5 in which the presence of NbO_2 and Nb_4O_5 might be associated with the partial reduction of Nb_2O_5. The presence of these lower oxides (NbO_2 and Nb_4O_5) got increased when longer holding time (10, 15 h) were employed at 600 ^oC as observed in figure 4.1. The increment in volume fraction of lower oxides can be correlated to the availability of sufficient time to reduce Nb_2O_5 resulting NbO_2 and Nb_4O_5 [1].

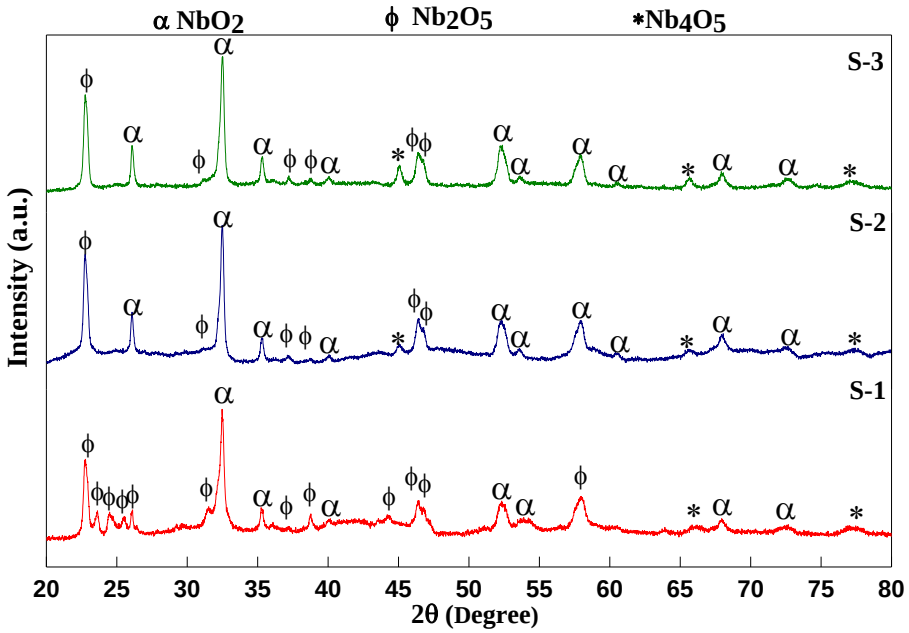

Figure 4.1: XRD pattern of all the samples (S-1, S-2 and S-3) synthesized at 600 °C with 2.0g Mg.

Synthesis temperature 700 °C: As an effect of synthesis temperature, the mixture of reactants was heated to 700 ^{o}C with the holding time of 5, 10 and 15 h denoted as sample S-4, S-5 and S-6, respectively as shown in figure 4.2. These XRD spectra consist several broad humps depicting the presence of amorphous humps along with the crystalline lower oxides of Nb (NbO_2 and Nb_4O_5). An increasing trend has also been observed in the crystallinity of Nb_2O_5 and NbO_2 as the holding time has increased at 700 °C.

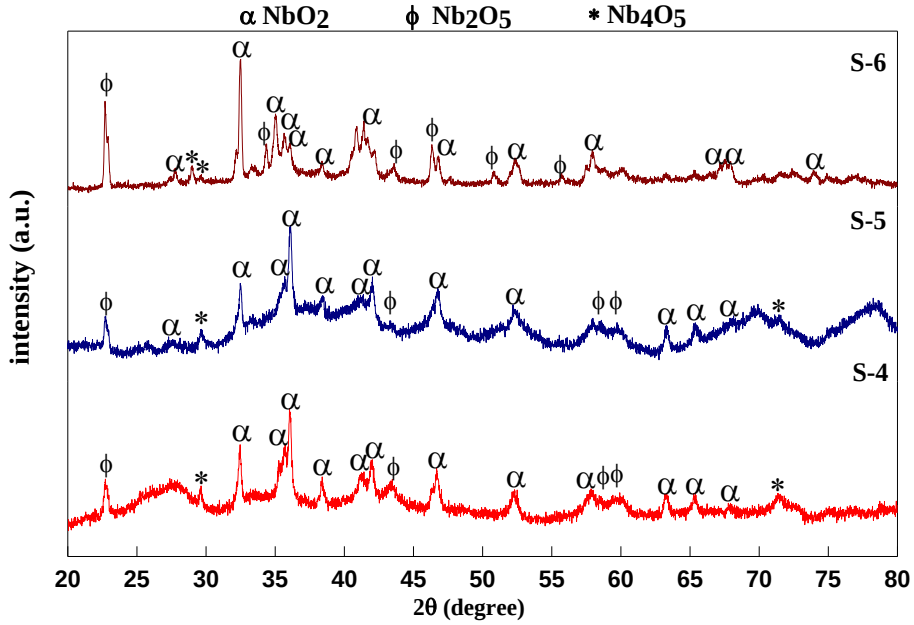

Figure 4.2: XRD pattern of all the samples (S-4, S-5 and S-6) synthesized at 700 °C with 2.0g Mg.

Synthesis temperature 800°C: After obtaining less crystalline diffraction peaks and amorphous background, the reactant mixture was heated at 800 °C with same holding time (5, 10 and 15h) denoted as S-7, S-8 and S-9, respectively as shown in figure 4.3. Similar to the XRD patterns obtained at 700 °C, S-7, S-8 and S-9 also possess amorphous humps with broadened diffraction peaks in all the samples. S-7 contains NbO_2 as major phase and Nb_2O_5 as minor phase. While, 10 h holding at 800 °C (S-8) resulted to the formation of NbB along with the reduction in Nb_2O_5 and NbO_2. Further, increment in holding time to 15 h led to the reduction of Nb_2O_5 content associated to the transformation of Nb_2O_5 to NbO_2.

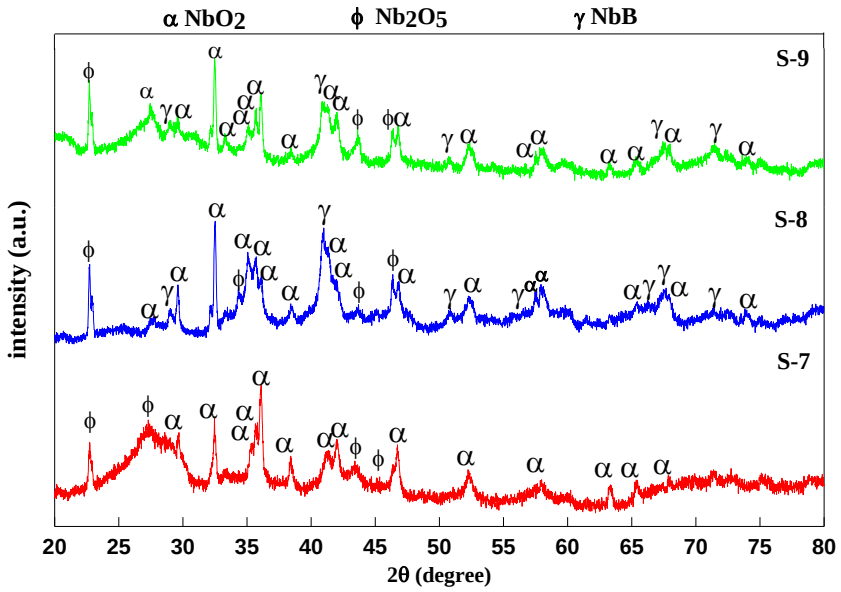

Figure 4.3: XRD pattern of all the samples (S-7, S-8 and S-9) synthesized at 800 °C with 2.0g Mg.

In all above discussed set of experiments, the partial reduction reaction is associated to either unavailability of thermal energy or insufficient amount of reducing agent i.e. Mg metal powder. Although the volume fraction of lower oxides along with signature of NbB were obtained at 800 ^oC as compared to 700 ^oC, however the presence of diffraction peaks corresponding to NbB in S-8 and S-9 provided a breakthrough for the optimization of amount of reactions instead of temperature and time.

B. Moderate Mg content (2.5g)

In 2nd set of experiments, keeping same amount of Nb_2O_5 and borax, the amount of magnesium metal powder was increased to 2.5g which makes the molar ratio to 1:20.5:1. Due to the presence of well crystalline peaks of Nb_2O_5 and NbO_2 in 5 h holding at 600, 700 and 800 ^oC, only 10 and 15 h holding was practiced at all the temperatures mentioned above to study the effect of amount of reducing agent.

Synthesis temperature 600 °C: At 600 °C, 10 h holding (sample S-10) was employed, which showed the presence of Nb_2O_5, NbO_2 along with NbB_2 as shown in figure 4.4. While, the prolonged holding time (15h) at 600 °C led to oxidation of products obtained in S-10 as observed in XRD pattern of S-11 (figure 4.4). In both the samples (S-10 and S-11), diffraction peaks are very broad with less intensity depicting the initiation of phase formation.

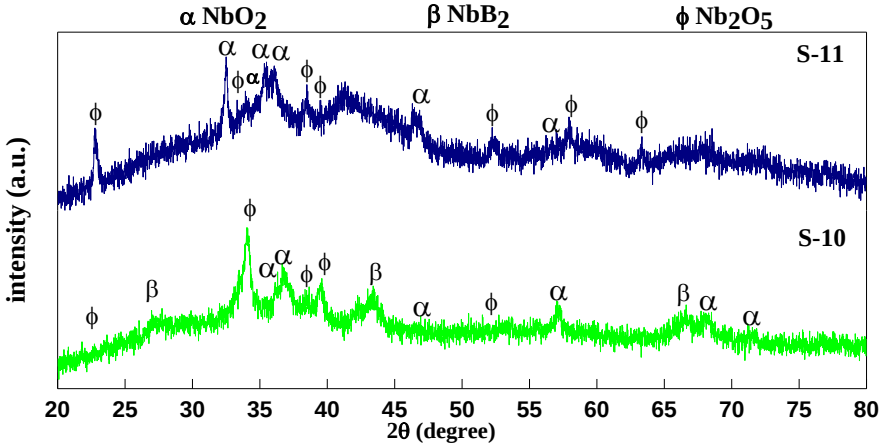

Figure 4.4: XRD pattern of all the samples (S-10, S-11) synthesized at 600 °C with 2.5g Mg.

Synthesis temperature 700 °C: Figure 4.5 shows the diffraction spectrum of sample S-12 and S-13 which were synthesized at 700 °C with 10 and 15h holding time, respectively. Contrary to results obtained at 600 °C, NbO_2 was obtained as major phase in S-12 and a broad hump was also observed corresponding to NbB_2 which might be associated to the very small crystallite NbB_2. Further, these crystallites have grown with respect to time at 700 °C which was confirmed in S-13 with enhanced volume fraction of NbB_2, diffraction peaks associated to NbO_2 have also been diminished (marked as α in figure 4.5). Which also supported the reduction boronization of Nb_2O_5.

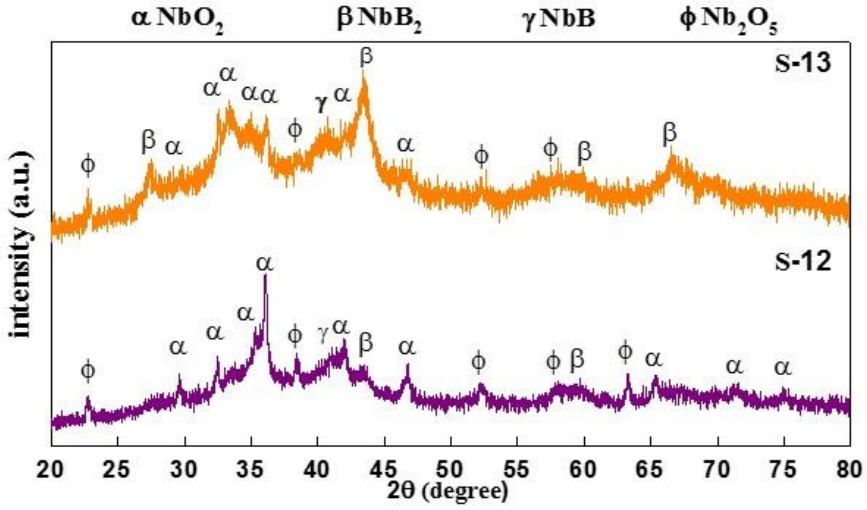

Figure 4.5: XRD pattern of all the samples (S-12, S-13) synthesized at 700 °C with 2.5g Mg.

Furthermore, at 800 ^{o}C, well crystalline multi-phase XRD spectrum were obtained with holding time 10 h and 15 h as shown in figure 4.6. As a result of 10 h holding at 800 ^{o}C (S-14), a mixture of NbO_2, Nb_2O_5, NbB and NbB_2 was obtained in which volume fraction of NbB_2 and NbB was not that much less as obtained in sample S-10 to S-13. Moreover, phase transition of NbO_2 and Nb_2O_5 was also observed. While, increased holding time (15 h) in sample S-15 resulted to the decrement in the content of NbO_2 and Nb_2O_5.

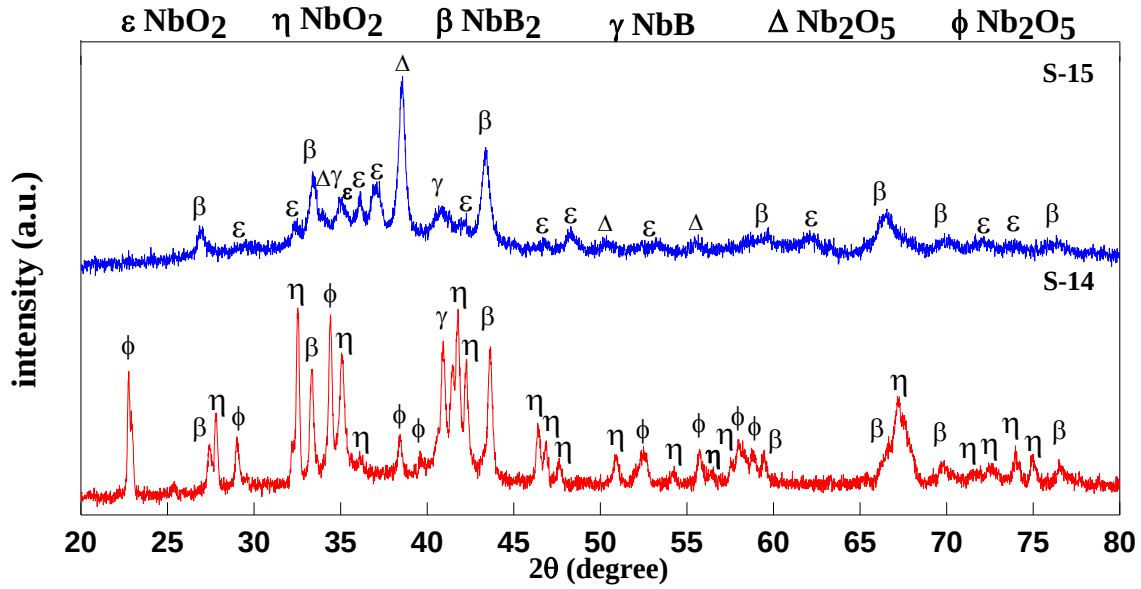

Figure 4.6: XRD pattern of all the samples (S-14, S-15) synthesized at 800 °C with 2.5g Mg.

C. High Mg content (3.5g)

After obtaining mixed phase samples, in the 3rd set of experiments containing higher amount of Mg i.e. 3.5g experiment was performed to facilitate the complete reduction of Nb_2O_5 resulting NbB_2 at same conditionds.

Synthesis temperature 600 °C: With higher content of Mg, longer holding time (10 and 15h) at 600°C resulted amourphous XRD pattern consisting 4 broad humps associated to NbO_2 and broadness revealed the highly distorted or very small crystals of NbO_2 as shown in figure 4.7. As compared to previous samples synthesized at 600 °C (S-1 to S-3, S-10, S-11), sample S-16 and S-17 comprised single phase NbO_2 which might be due to the availability of excess reducing agent (Mg) to reduce Nb_2O_5 at low temperature (600 °C) along with the absence of any signature of boronization in the samples.

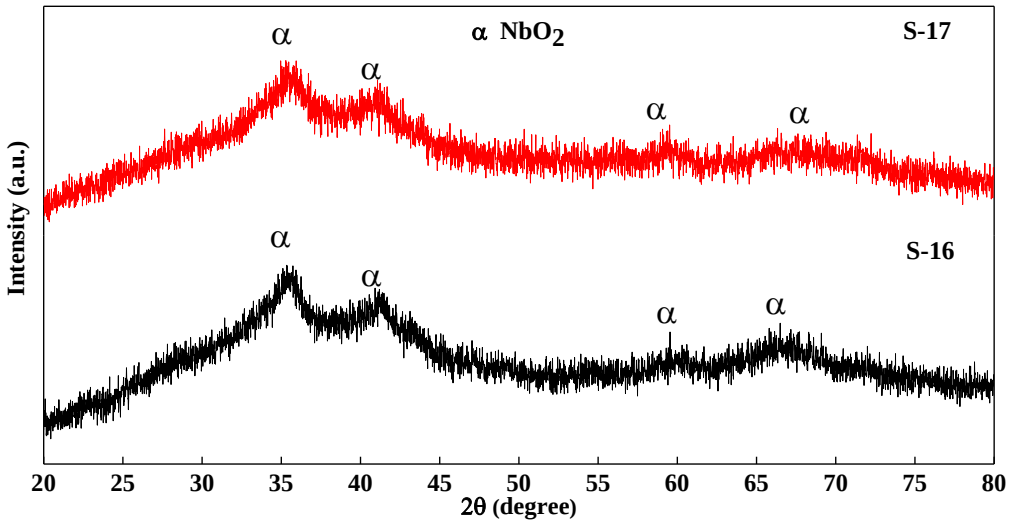

Figure 4.7: XRD pattern of all the samples (S-16, S-17) synthesized at 600 °C with 3.5 g Mg.

Synthesis temperature 700 °C: Figure 4.8 shows the XRD patterns of the samples S-18, S-19 and S-20 depicting the presence of NbB_2 (major) and NbB (minor) at 5, 10 and 15h holding at 700 °C respectively. The formation of NbB_2 and NbB without any signature of lower oxides (NbO_2, Nb_4O_5) asserted to the complete reduction of Nb_2O_5 followed by boronization.

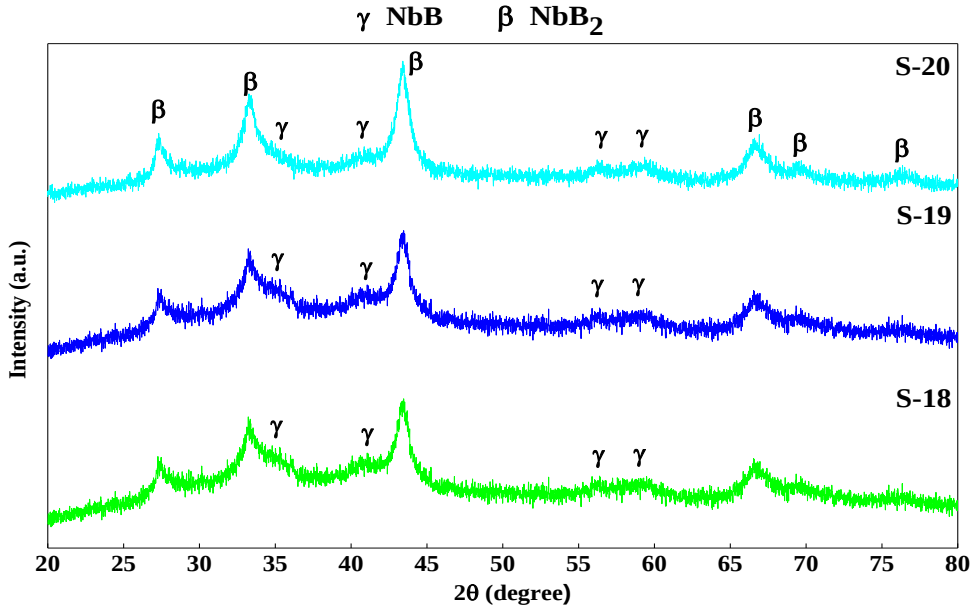

Figure 4.8: XRD pattern of all the samples (S-18, S-19 and S-20) synthesized at 700 °C with 3.5g Mg.

Moreover, these two physical processes are occurring simultaneously which might be due to *in-situ* synthesis process. Further, as an effect of holding time at 700 °C, the crystallinity of

NbB_2 tends to increase due to the incorporation of B to Nb atom resulting better growth in longer holding.

Synthesis temperature 800 °C: Even higher temperature 800 °C with same set of holding time resulted in the formation of NbB_2 as shown in figure 4.9. Sample S-21 showed the formation of NbB_2 as major phase along with the reduced Nb_2O_5 and NbO_2 which might be corroborated to the insufficient time (5h) at 800 °C to reduce and boronize Nb_2O_5. Further, increment in the holding time to 10 h resulted to the complete reduction of Nb_2O_5 and partial boronization of Nb showing NbB_2 (major) and NbB (minor). It is well known principle that longer holding promotes the diffusion pnehomenon which was observed in prolonged holding (15 h) at same temperature with the diffraction peaks related to NbB_2 (sample S-23) [2]. Such transformation might be associated to the completion of reduction and boronization of Nb_2O_5.

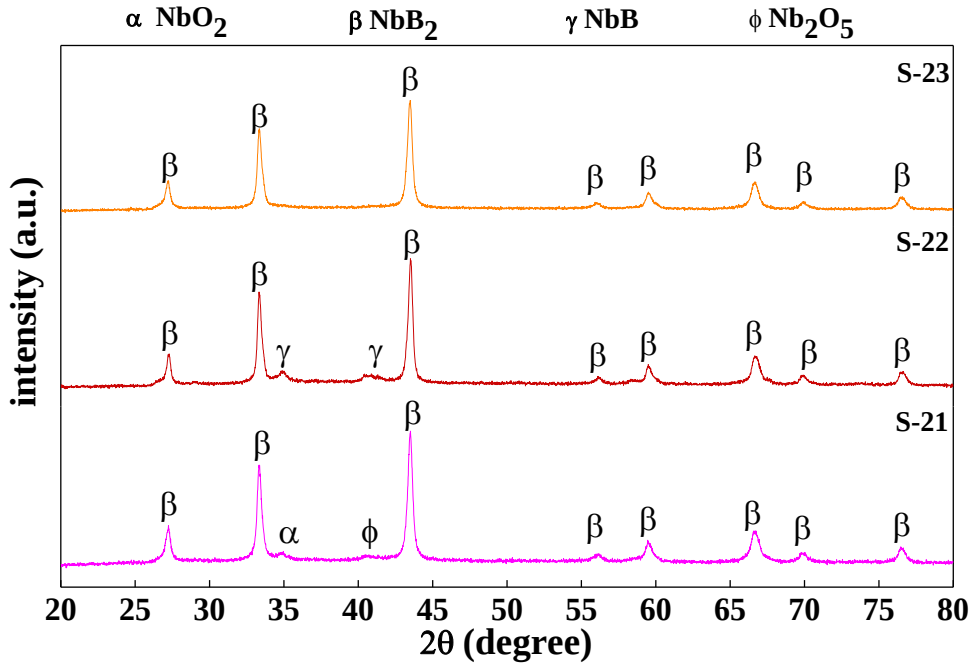

Figure 4.9: XRD pattern of all the samples (S-21, S-22 and S-23) synthesized at 800 °C with 3.5g Mg.

Based on the XRD results of all the synthesized samples, it can be simulated that the role of reducing agent (Mg) is very critical along with the synthesis temperature and holding time. As an effect of synthesis temperature, thermal energy is the only governing parameter which manuever the chemical reaction. Moreover, the holding time at fixed temperature governs the diffusion process leading to more reduced products at longer holding time. While, amount of Mg controls the rate of chemical reaction as a function of thermal energy and rate of reaction which can be easlity interpreted by varying the amount of Mg in same holding time at fixed temperature as observed in sample S-9, S-15 and S-23. 2.0g Mg contributed to the partial

reduction of Nb_2O_5 forming the mixture of Nb_2O_5 and NbO_2+NbB (figure S-9) and 2.5g Mg enhanced the extent of reduction of Nb_2O_5 by showing the formation of orthorhombic-Nb_2O_5 (ϕ) from monoclinic -Nb_2O_5 (Δ), tetragonal-NbO_2, NbB and NbB_2 (figure 4.6). Moreover, 3.5g Mg supported the single step formation of single phase NbB_2 (figure 4.9) by enhancing the rate of reduction and boronization of Nb_2O_5.

3.3 Williamson-Hall analysis

X-ray line profile analysis of all the samples shows that the size and distortion in it. Scherrer formula is the most useful mathematical formula to measure crystallite size which is related to the full width at half maximum (FWHM;β_{hkl}) which is given below:

$$t = \frac{k\lambda}{\beta_{hkl}\cos\theta_{hkl}} \tag{4.1}$$

where $k\,(\text{shape factor}) = 2\sqrt{\ln(2)\pi} \sim 1$; θ: Bragg angle; λ: X-ray wavelength (~0.15406 nm). The crystallite size is completely responsible for peak broadening, but Stokes and Wilson provided the mathematical relation between peak broadening due to strain [3]

$$\beta = 4.\varepsilon.\tan\theta_{hkl} \tag{4.2}$$

The combination of equation (2) and (3) represent the Williamson-Hall models, are useful to extract the individual effects of size and strain, can be expressed as follows:

(A) Uniform Strain Model (USM)

$$\beta_{hkl}\cos\theta_{hkl} = \frac{k\lambda}{t} + 4.\varepsilon\sin\theta_{hkl} \tag{4.3}$$

Uniform distribution of strain throughout the crystal is main assumption of USM model. Due to which slope of linear fit of Williamson-Hall plot ($\beta_{hkl}\cos\theta_{hkl}$ vs. $4\sin\theta_{hkl}$) provides the strain (ε) and measure the crystallite size (t) by intercept$\left(=\frac{k\lambda}{t}\right)$.

But in the most of the cases, nanomaterials do not follow the above condition of strain homogeneity and criteria of homogeneous stress and homogeneous strain energy provide more logical results [4]

(B) Uniform Stress Deformation Model (USDM):

$$\beta_{hkl}\cos\theta_{hkl} = \frac{k\lambda}{t} + \frac{4\sigma\sin\theta_{hkl}}{E_{hkl}} \tag{4.4}$$

(C) Uniform Strain Energy Density Model (USEDM):

$$\beta_{hkl}\cos\theta_{hkl} = \frac{k\lambda}{t} + 4\sin\theta_{hkl}\left(\frac{2u}{E_{hkl}}\right)^{\frac{1}{2}} \tag{4.5}$$

For the hexagonal system, elastic moduli [5] for the plane (hkl)

$$E_{hkl} = \frac{\left[h^2 + \frac{(h+2.k)^2}{3} + \left(\frac{a.l}{c}\right)^2\right]^2}{s_{11}\left(h^2 + \frac{(h+2.k)^2}{3}\right)^2 + s_{33}\left(\frac{a.l}{c}\right)^4 + (2.s_{13} + s_{44})\left[h^2 + \frac{(h+2.k)^2}{3}\right]\left(\frac{a.l}{c}\right)^2}$$

where s_{11} = 1.9178 × 10^{-3} GPa, s_{12} = 0.1064 × 10^{-3} GPa, s_{13} = 0.7633 × 10^{-3} GPa, s_{33} = 2.9212 × 10^{-3} GPa and s_{44} = 4.5454 × 10^{-3} GPa [6]. To calculate strain, Hook's law ($\sigma = \varepsilon E_{hkl}$) and strain energy $\left(u = \frac{1}{2}\varepsilon^2 E_{hkl}\right)$ was used in USDM and USEDM models, respectively as shown in figure (4.10-4.12) for the synthesized samples at different holding time at 700 and 800 °C in which NbB_2 is present. Separation of the contribution of size and strain in the broadening of diffraction peaks allows the dependency of β_{hkl} on tanθ instead of $(\cos\theta)^{-1}$ [7].

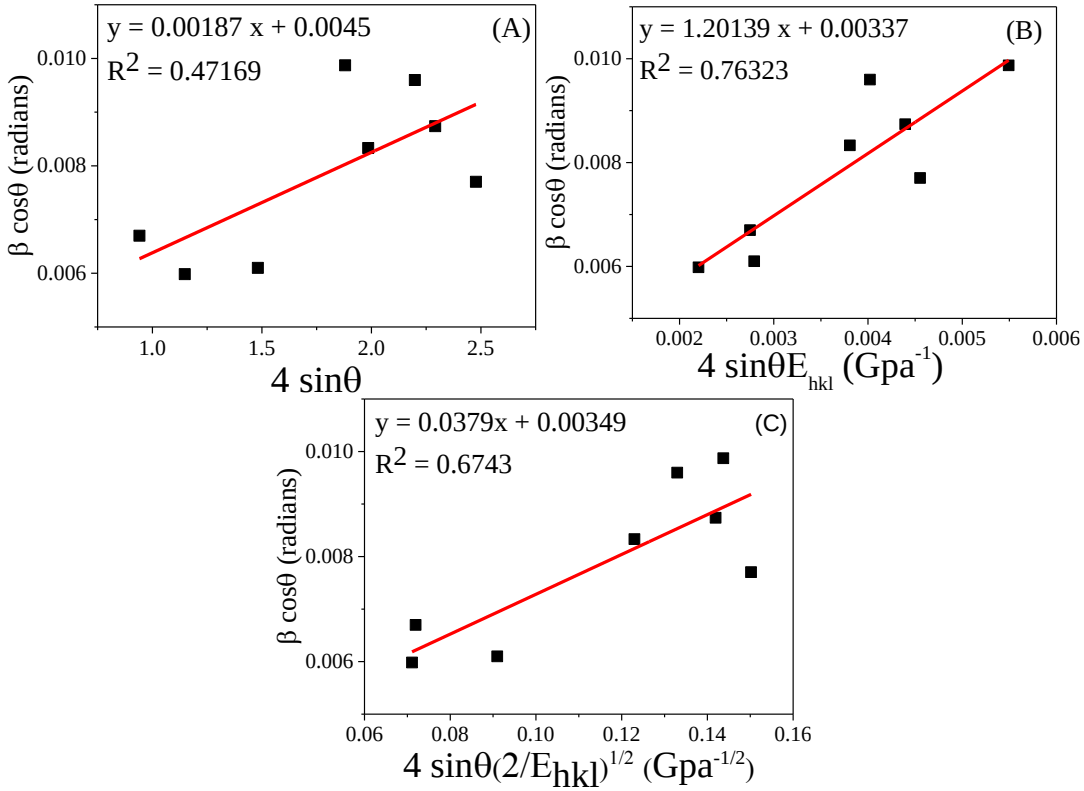

Figure 4.10: The W-H analysis of S-21, the crystalline size is extracted from the y-intercept of the fit. The strain, stress and deformation strain energy density is extracted from the slope (A) USM, (B) USDM and (C) USEDM.

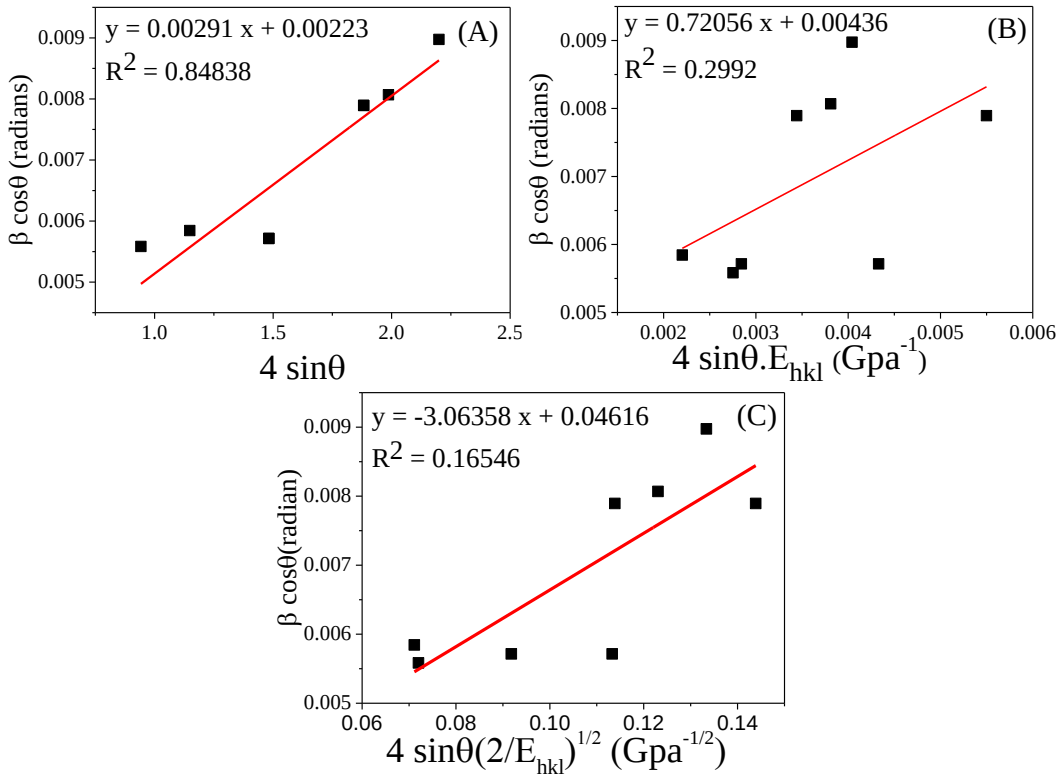

Figure 4.11: The W-H analysis of S-22, the crystalline size is extracted from the y-intercept of the fit. The strain, stress and deformation strain energy density is extracted from the slope (A) USM, (B) USDM and (C) USEDM.

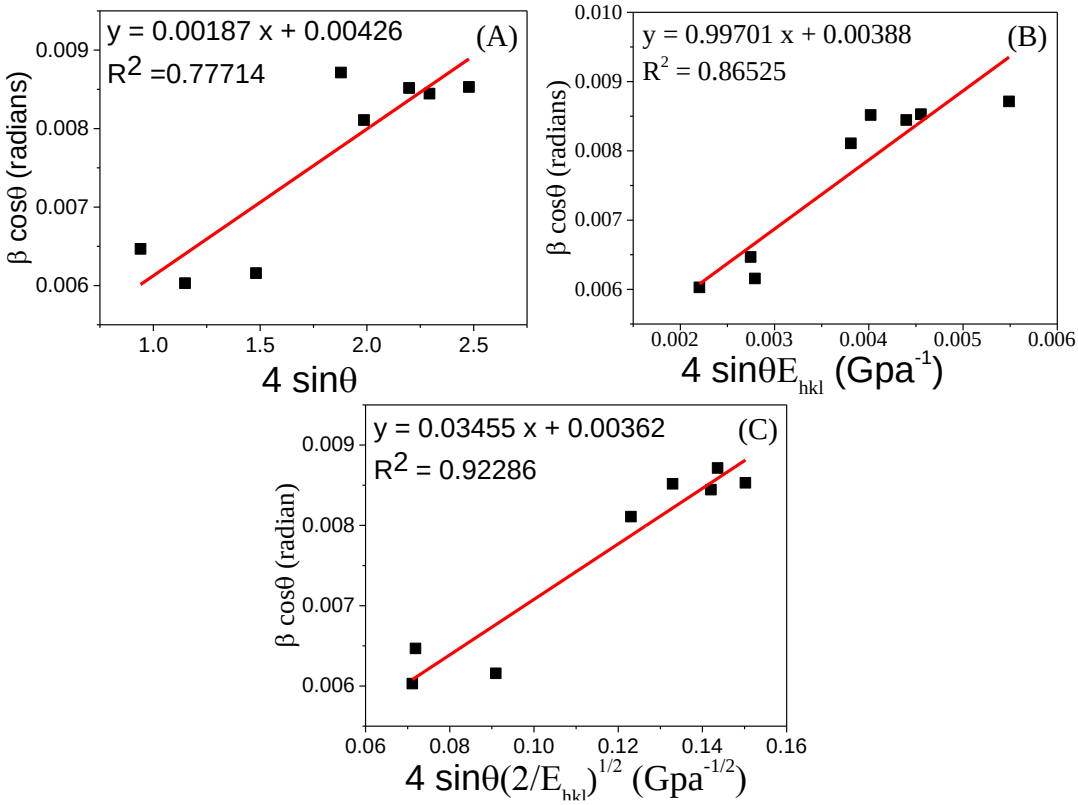

Figure 4.12: The W-H analysis of S-23, the crystalline size is extracted from the y-intercept of the fit. The strain, stress and deformation strain energy density is extracted from the slope (A) USM, (B) USDM and (C) USEDM.

Table 4.2: Williamson-Hall analysis of all synthesized samples.

S. Id	USM			USDM				USEDM				
	ε $\times 10^{-3}$	t nm	R^2	ε $\times 10^{-3}$	σ GPa	t nm	R^2	ε $\times 10^{-3}$	σ GPa	u $\times 10^{3}$ kJm^{-3}	t nm	R^2
S-21	1.87	32.5	0.47	2.58	1.21	42.9	0.76	2.45	1.17	1.74	41.5	0.87
S-22	2.07	41.3	0.84	1.96	0.98	38.3	0.68	2.31	1.11	1.69	46.1	0.89
S-23	1.87	32.5	0.77	2.14	1.01	37.3	0.86	2.25	1.08	1.21	39.9	0.92

As calculated from W-H analysis, USDEM model fits the sample data more appropriately (higher value of R^2 in each sample) as compared to the other two models (USM and USDM) suggesting uniformity of strain deformation energy throughout the synthesized nanoparticles as shown in table 4.2. In USM model, S-22 showed the best fit value of R^2 (0.84) signifying the better uniformity of strain (USM) in the crystal than other samples. While, S-23 possessed uniform strain deformation energy density (USDEM, R^2=0.92) as compared to other synthesized samples. Being single phase, S-23 possess least distortion in the lattice while, presence of lesser boron in lattice caused more distortion in a sequence as follows S-23<S-22<S-21. The variation in strain and distortion energy indicated that during the formation of NbB_2 at 800 °C, diffusion of boron was promoted by increasing the holding time thus incorporating the equilibrium configuration of NbB_2.

4.3. Thermal analysis

Thermal stability of synthesized single phase NbB_2 (S-23) was determined by TGA/DSC analysis from room temperature to 800 °C at a heating rate of 10 °C/min in air atmosphere. Figure 4.13 shows the TG, DTG and DSC curve of S-23 in which very small weight loss has been observed upto 300 °C associated to removal of adsorbed water or surface contamination [1]. From 300-450 °C, slow mass gain was observed with a exothermic DSC signal which might be associated to the adsorption of oxygen on the surface of nanoparticles. This mass gain has become rapid till 600 °C has achieved which signifies the exothermic oxidation of boron and niobium resulting niobium oxide and boron oxide [8, 9]. The oxidation of two elements (Nb and B) is confirmed by double DTG signals corresponding to oxidation of boron (centered 533 °C) and niobium (centered 566 °C) as shown in figure 4.13 and will be discussed in section 'microstructure analysis'. Further, increase in the temperature upto 800 °C resulted in complete oxidation of sample suggested by the constant line in thermogram.

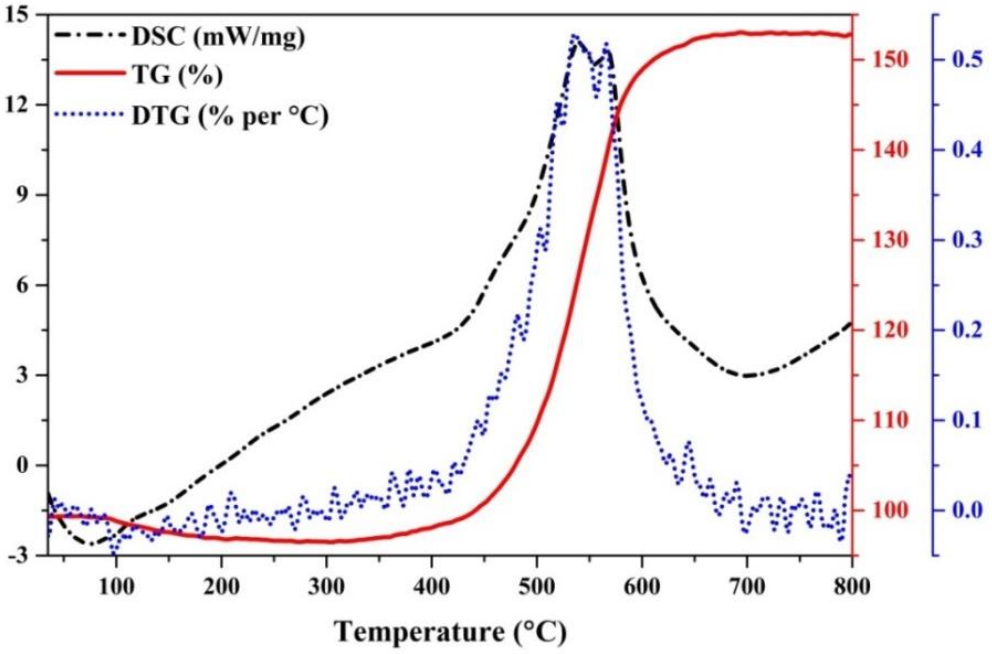

Figure 4.13: Thermal (TG, DSC and DTG) analysis of sample 'S-23'.

4.4. Microstructural analysis

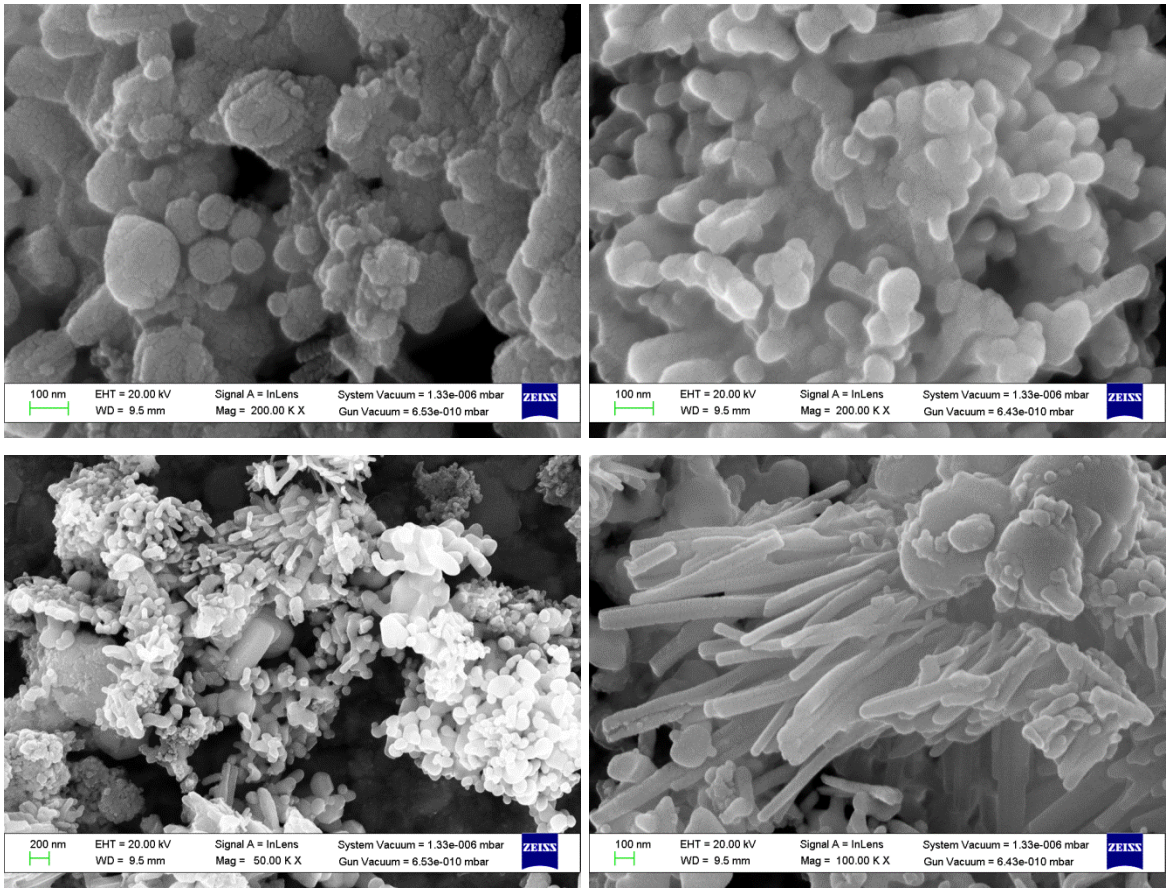

Figure 4.14: FE-SEM micrographs of single phase NbB_2 (S-23) samples which shows the agglomeration of nanoparticles forming nanorod morphology.

Figure 4.14 shows the FE-SEM microstructure of single phase NbB_2 nanoparticles (S-23). The as-synthesized sample has non-faceted morphology with a tendency to grow in rod like structure as shown in figure 4.14, but aggregates of spherical and non-spherical particles are clearly visible having an average thickness of rods 60-70nm. Further, figure 4.15 confirmed the agglomeration of nanoparticles through TEM microstructures of S-23 having coated morphology of NbB_2 nanoparticles.

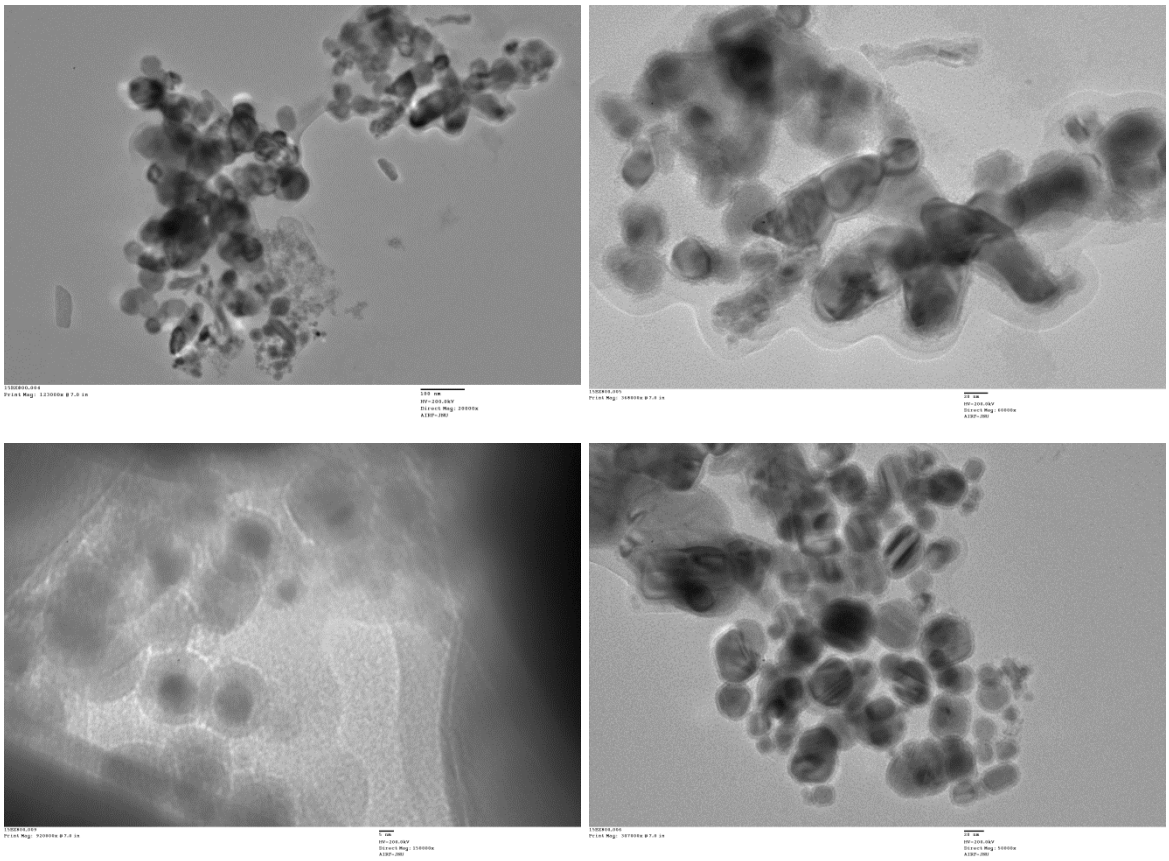

Figure 4.15: TEM micrographs of sample S-23 asserting the coated NbB_2 nanoparticles similar to figure 4.14; and inclining to attain nano rod-like shape.

The mean particle size on calculated from TEM micrographs with broad distribution of particles is nearly 37.8 nm. Therefore, logarithmic particle size is more advantageous than normal particle size to analyze frequency vs. size plot as shown in figure S-23. Following lognormal distribution function was used to calculate the frequency of nanoparticles

$$f(s) = \frac{1}{\sqrt{2\pi}.\sigma.s_i} e^{-\left(\frac{(\log(s_i)-\mu)^2}{2\sigma^2}\right)} \tag{4.6}$$

where $\mu = \frac{\sum \log(s_i)}{\sum n_i}$; and $\sigma = \sqrt{\frac{\sum(\log(s_i)-\mu)^2}{\sum n_i}}$ (4.7)

where f(s) denotes the lognormal distribution function, s_i represents the size of i^{th} particle of NbB_2, $\sum n_i$ is the total number of particles, mean diameter (μ) and standard deviation (σ) of particle size.

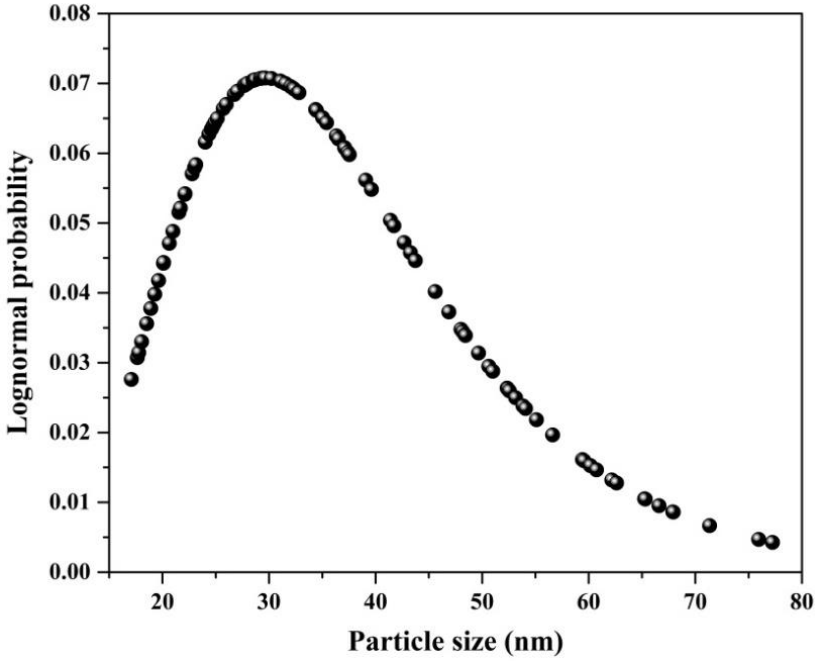

Figure 4.16: Lognormal distribution of particle size of sample S-23 nanoparticles.

4.5. Proposed synthesis mechanism

In order to understand the reaction mechanism responsible for the formation of NbB_2 nanoparticles at low temperature, it is prerequisite to infer the role of reactants. Borax ($Na_2B_4O_7.10H_2O$) is one of the most common chemical being used in household purposes. It contains 8 mole of adsorbed and 2 mole of crystal molecules of H_2O. Moreover, it is well studied fact that borax can be dehydrated at 600 °C [10] inducing huge vapor pressure inside the autoclave during heating as shown in Equation (x).

$$Na_2B_4O_7.10H_2O \xrightarrow{\sim 150℃} Na_2B_4O_7.2H_2O \xrightarrow{\sim 600℃} Na_2B_4O_7 \tag{4.8}$$

In closed autoclave, high vapor pressure reduces the reaction temperature. Mg reduces Nb_2O_5 and anhydrous borax ($Na_2B_4O_7$) resulting NbO_2 and mixture of Na_2O, B_2O_3 and MgO as shown in figure 4.17a. For all the chemical reactions, negative values of heat of formation (ΔH_f) indicate the exothermic reaction and is calculated with the help of following relation;

$$\Delta H_f = \int_{298}^{T} C_p dT = \Delta a.\Delta T + \Delta b.\Delta T^2 + \Delta c.\Delta T^{-1} \tag{4.9}$$

Where Δa, Δb and Δc are the difference of heat capacities of products and reactants of chemical reaction. The formation of NbO_2 from Nb_2O_5 is confirmed with the help of XRD analysis at 600 °C (sample S-16). Among all the possible reduction reactions (mentioned below), it is very much elucidated that thermal decomposition of $Na_2B_4O_7$ is quite feasible along with the reduction of Nb_2O_5 providing the mixture of NbO_2, Na_2O, B_2O_3 and B. While, reduction of borax and Nb_2O_5 in the presence of Mg and B_2O_3 is not feasible with positive ΔH as shown in figure 4.17a.

$$Nb_2O_5 + Mg + Na_2B_4O_7 \rightarrow 2NbO_2 + Na_2O + 2B_2O_3 + MgO \quad (4.10)$$

$$Na_2B_4O_7 \rightarrow Na_2O + 2B_2O_3 \quad (4.11)$$

$$Nb_2O_5 + 4Mg + Na_2B_4O_7 \rightarrow 2NbO_2 + Na_2O + B_2O_3 + 4MgO + 2B \quad (4.12)$$

$$Nb_2O_5 + Mg \rightarrow 2NbO_2 + MgO \quad (4.13)$$

Further, the reduction of either NbO_2 or remaining Nb_2O_5 to result in the formation of NbB_2 requires more energy as compared to a simultaneous reduction of the mixture of Nb_2O_5 and $Na_2B_4O_7$ as the magnitude of heat of formation is higher for the latter condition (figure 4.17b). While, the presence of Mg in autoclave led to the reduction of $Na_2B_4O_7$ resulting the decomposition of borax to Na_2O, B and MgO. The resulting nascent boron and remaining Mg reduce Nb_2O_5/NbO_2 to produce NbB_2, B_2O_3 and MgO which can be expressed as following equations;

$$Nb_2O_5 + 2Mg + 6B \rightarrow 2NbB_2 + 2MgO + B_2O_3 \quad (4.14)$$

$$Nb_2O_5 + 5Mg + 4B \rightarrow 2NbB_2 + 5MgO \quad (4.15)$$

$$2NbO_2 + Mg + 6B \rightarrow 2NbB_2 + MgO + B_2O_3 \quad (4.16)$$

$$NbO_2 + 2Mg + 2B \rightarrow NbB_2 + 2MgO \quad (4.17)$$

As a result of Equation xiv, boron as a by-product forms a coating of Nb_2O_5 particles and along with Mg reduce to form NbB_2 as explained by Equation (4.14-4.17). Such coated NbB_2 nanoparticles were observed in TEM analysis (Figure 4.15). Moreover, these synthesized nanoparticles have a tendency to join each other to attain rod-like morphology as observed in FE-SEM (Figure 4.14). Further, basic oxides (MgO, Na_2O and B_2O_3) were removed with the help of HCl leaching (1:1) resulting $MgCl_2$, NaCl and BCl_3 which are soluble in H_2O. Hence, these can be removed by washing with distilled H_2O.

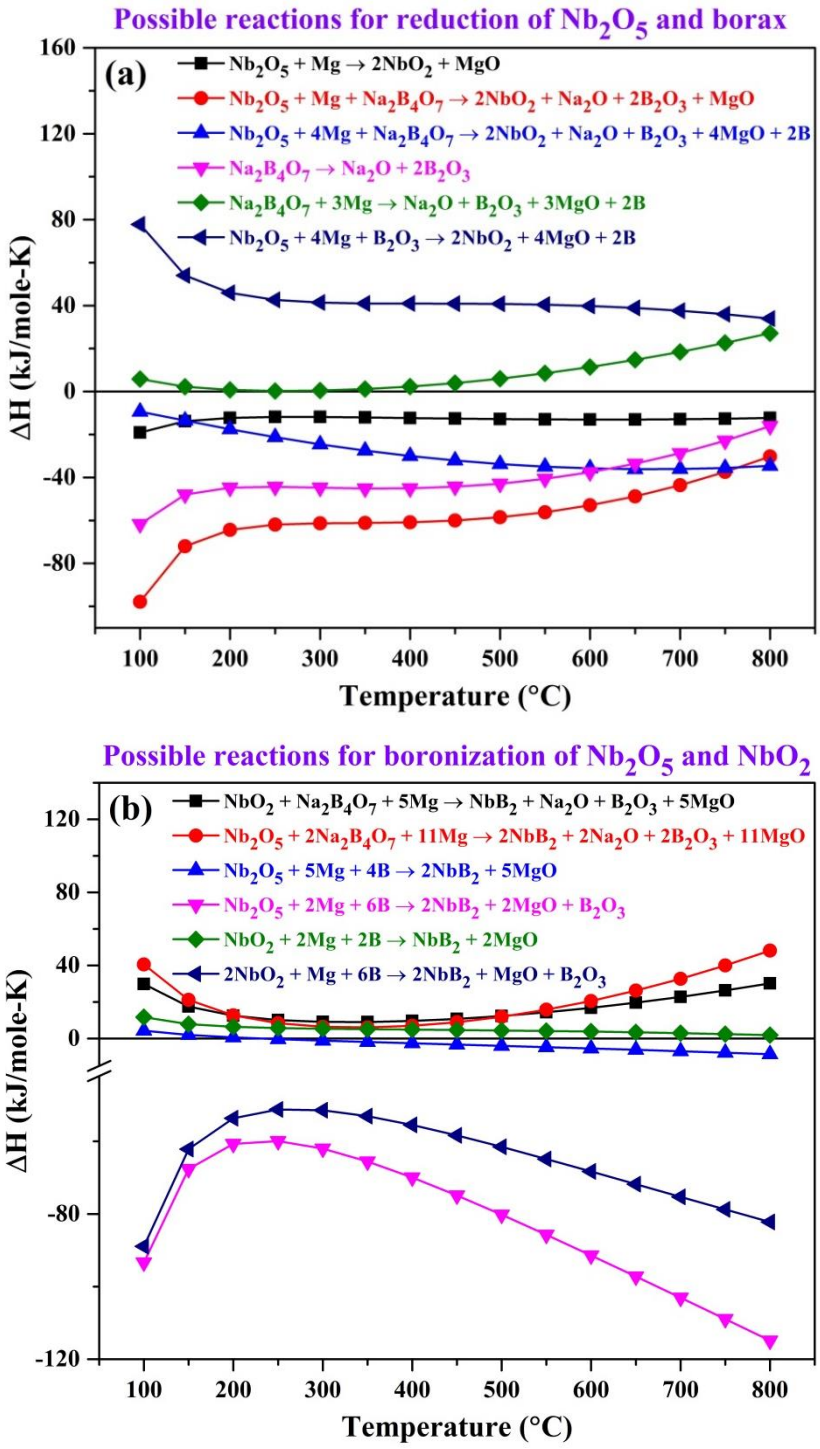

Figure 4.17: Temperature dependent heat of formation for (a) reduction of Nb_2O_5, borax and (b) *in-situ* reduction-boronization of Nb_2O_5, NbO_2 resulting NbB_2.

References

[1] A. Gupta, G. Singla, O.P. Pandey, Effect of synthesis parameters on structural and thermal properties of NbC/C nano composite synthesized via in-situ carburization reduction route at low temperature, Ceram. Int. 42 (2016) 13024–13034.

[2] T.Y. Kosolapova, Carbides: properties, production and applications, Plenum Press, NewYork-London (1971).

[3] S. Vives, E. Gaffet, C. Meunier, X-ray diffraction line profile analysis of iron ball milled powders, Mater. Sci. Eng. A. 366 (2004) 229–238.

[4] G. Singla, K. Singh, O.P. Pandey, Williamson-Hall study on synthesized nanocrystalline tungsten carbide (WC), Appl. Phys. A Mater. Sci. Process. 113 (2013) 237–242.

[5] J.M. Zhang, Y. Zhang, K.W. Xu, V. Ji, General compliance transformation relation and applications for anisotropic cubic metals, Mater. Lett. 62 (2008) 1328–1332.

[6] C.F. Cline, H.L. Dunegan, G.W. Henderson, Elastic constants of hexagonal BeO, ZnS, and CdSe, J. Appl. Phys. 38 (1967) 1944–1948.

[7] A. Khorsand Zak, W.H. Abd. Majid, M.E. Abrishami, R. Yousefi, X-ray analysis of ZnO nanoparticles by Williamson-Hall and size-strain plot methods, Solid State Sci. 13 (2011) 251–256.

[8] J. Ma, Y. Du, M. Wu, G. Li, Z. Feng, M. Guo, Y. Sun, W. Song, M. Lin, X. Guo, A simple inorganic-solvent-thermal route to nanocrystalline niobium diboride, J. Alloys Compd. 468 (2009) 473–476.

[9] A. Kılıçarslan, F. Toptan, I. Kerti, S. Piskin, Oxidation of boron carbide particles at low temperatures, Mater. Lett. 128 (2014) 224–226.

[10] A. Ekmekyapar, A. Baysar, A. Kunkul, Dehydration kinetics of tincal and borax by thermal analysis, Ind. Eng. Chem. Res. 36 (1997) 3487–3490.

5. Conclusion

On the basis of the performed experiments, it can be asserted that the formation of single phase NbB_2 has been achieved at 800 °C with 15h holding by using 3.5g Mg and 2g borax ($Na_2B_4O_7.10H_2O$) powder. As a result of chemical reactions with 2.0g Mg, little signature of NbB was observed in sample S-8, S-9 and rest other samples (S-1 to S-7) contained the mixture of Nb_2O_5 and NbO_2 associated with the partial reduction of Nb_2O_5. While, higher Mg content (2.5g) showed the more feasibility of the formation of NbB_2 in samples S-10, S-12 to S-15. Further, higher Mg content (3.5g) resulted single step formation of NbB_2 nano powder. Along with the optimization of amount of reducing agent (Mg), optimization of holding time was very critical as observed the oxidation of NbB_2 in S-11.

Based on XRD analysis, it can be established that the formation of NbB_2 from Nb_2O_5 is not a direct chemical reaction but, it is an *in-situ* reduction-boronization process which includes intermediate steps, provided as follows;

$$Nb_2O_5 \rightarrow NbO_2 \rightarrow Nb_4O_5 \rightarrow NbB \rightarrow NbB_2$$

Further, with the help of TGA/DSC analysis, it can be concluded that the single phase NbB_2 (S-23) nanoparticles are stable upto 400°C. Morphological observations suggested the formation of nano NbB_2 rods by joining NbB_2 nanoparticles with a fine coating with ~30nm average particle size. Based on the thermodynamic calculations, combine reduction of Nb_2O_5 and $Na_2B_4O_7$ is more feasible than individual resulting formation of nascent boron which further boronize Nb-oxides (Nb_2O_5 and NbO_2) to result the formation of nano NbB_2.

6. Future scope

Based on result obtained in present work, various source of Nb, B and reducing agents can be used to synthesize NbB_2 at nanoiscale. Moreover, effect of synthesis parameters can be studied in terms of distortion in the lattice with the help of Williamson hall analysis which will provide a direct interpretation of stoichiometry of NbB_{2+x}.

By varying the reactants or synthesis routes morphological and structural features can be studied which further will be important for various mechanical, optical and magnetic properties. Being a refractory compound, its thermal stability at nano scale play a very critical role in altering various automobile, aerospace and nuclear power plant applications.